NANO · MICRO small
www.small-journal.com

2D Arsenene and Arsenic Materials: Fundamental Properties, Preparation, and Applications

*Yi Hu, Junchuan Liang, Yuren Xia, Cheng Zhao, Minghang Jiang, Jing Ma, Zuoxiu Tie, and Zhong Jin**

As emerging 2D materials, arsenene and arsenic materials have attracted rising interest in the past few years. The diverse crystalline phases, exotic electrical characteristics, and widespread applications of 2D arsenene and arsenic bring them great research value and utilization potential. Herein, the recent progress of 2D arsenene and arsenic is reviewed in terms of fundamental properties, preparation, and applications. The fundamental properties of 2D arsenene and arsenic, including the crystal phases, environmental stability, and electrical structure, from theoretical to experimental reports are first summarized. Then, the experimental processes for preparing 2D arsenene and arsenic, along with their respective advantages and disadvantages, are introduced including epitaxial growth, mechanical exfoliation, and liquid-phase exfoliation. Moreover, applications of 2D arsenene and arsenic are discussed, suggesting a wide range of applications of 2D arsenene and arsenic in field-effect transistors, sensors, catalysts, biological applications, and so on. Finally, some perspectives about the challenges and opportunities of promising 2D arsenene and arsenic are provided. This review provides a helpful guidance and stimulates more focus on future explorations and developments of 2D arsenene and arsenic.

1. Introduction

Novel 2D materials, such as monoelemental 2D materials (graphene, silicene, germanene, borophene, phosphorene, etc.), boron nitride (BN), and metal chalcogenides (MoS_2, WS_2, $MoSe_2$, WSe_2, SnS_2, $Bi2Se_3$, etc.), have been extensively studied by researchers.[1–8] These 2D materials often exhibit distinguished chemical and physical properties, such as high anisotropy, large surface area-to-volume ratios, excellent mechanical properties, high thermal conductivity, tunable bandgaps, quantum spin Hall (QSH) effect, enhanced photoluminescence (PL), strong light–matter interactions, and ultrahigh surface sensitivity, making them attractive for investigating exotic physics and exploring a wide range of applications.[7–15] In particular, due to the high charge carrier mobility, good switching performance, and strong gate-controlled effects, 2D materials also show great potential in constructing new electronic devices, which are expected to be candidates for the next generation of semiconductor transistors.[1,16–19] Moreover, van der Waals (vdWs) interactions and dangling bond-free surfaces allow the refabrication of 2D heterostructures by stacking different 2D materials without the consideration of crystal lattice matching.[9,20–22] Recently, 2D group-VA materials (2D pnictogens), including phosphorene, arsenene, antimonene, and bismuthene, have also attracted significant research interest, and been investigated by various theoretical and experimental approaches.[5,6,23–31] 2D pnictogens possess various intriguing properties and can be employed for enormous applications ranging from electronics, electrochemistry, optoelectronics, sensors, catalysis, and energy storage to biology.[23,24,26–42]

2D arsenene and arsenic, as a member of 2D group-VA materials, were studied by many theoretical calculations. As a congener of phosphorene, 2D arsenene and arsenic have been precited to be a promising semiconductor when their thickness is reduced to few layers and their bandgaps are tuned by applying external strains.[45,47–49] It has also been demonstrated that functionalized arsenene (AsX, X = F, Cl, Br, I, OH, and CH_3) is a QSH insulator and possesses a nontrivial topological electronic state.[50–53] In addition, field-effect transistors (FETs) based on monolayer arsenene and antimonene simulated by the first-principles method exhibit good performance compliant with industry requirements.[54–56] Beyond theoretical calculations and simulations, in recent years, experimental studies have also been explored to uncover the fundamental features of 2D arsenene and arsenic. Mechanical exfoliation, liquid-phase exfoliation, and chemical vapor deposition have been successively applied to obtain arsenene or 2D arsenic materials.[30,38,39,46,57–62] Benefiting from the development of preparation strategies, the potential applications and exotic properties of arsenene or 2D arsenic materials are largely promoted and

Y. Hu, J. Liang, Y. Xia, C. Zhao, M. Jiang, J. Ma, Z. Tie, Z. Jin
MOE Key Laboratory of Mesoscopic Chemistry
MOE Key Laboratory of High Performance Polymer Materials and Technology
Jiangsu Key Laboratory of Advanced Organic Materials
School of Chemistry and Chemical Engineering
Nanjing University
Nanjing 210023, China
E-mail: zhongjin@nju.edu.cn
Y. Hu, J. Liang, Y. Xia, C. Zhao, M. Jiang, Z. Tie, Z. Jin
Shenzhen Research Institute of Nanjing University
Shenzhen 518063, China

The ORCID identification number(s) for the author(s) of this article can be found under https://doi.org/10.1002/smll.202104556.

DOI: 10.1002/smll.202104556

studied.[39,44,46,58–60,63–65] Moreover, the 2D arsenene and arsenic materials also demonstrated some of specificity with respect to other 2D materials. Both metallic phases and semiconductor phases of arsenic materials exist naturally, enabling a large flexibility to manipulate and construct various functional devices based on 2D arsenene, such as new-concept devices consisting entirely of arsenene. Layer-dependent metal-to-semiconductor transition is also a light spot of arsenene, enabling the control of conduction type of arsenene in a wide range. Especially, the 2D arsenene and arsenic materials show different toxicities toward cancer cells and normal cells, which is rarely discovered in other 2D materials.[48] Owing to the oxidizing species in cancer cells, the valence states of 2D arsenene and arsenic materials could be transferred from 0 to +3 in the cancer cells, while this effect is absent in normal cells.[39,66] As those outstanding features of 2D arsenene and arsenic materials and its studies move forward, it is expected that this novel material can complement the properties of current 2D materials and enrich the family of 2D materials. Although some articles have reviewed the theoretical and experimental developments of elemental 2D materials or group-VA 2D materials,[5,6,24–28,67–71] systematic reviews and prospects focused on 2D arsenene and arsenic are still absent and need to be complemented to accommodate their rapid developments.

Herein, we offer a comprehensive review on the recent theoretical and experimental advances of 2D arsenene and arsenic in terms of their intrinsic properties, crystal structure, experimental preparation, and applications (**Figure 1**). We first summarized the physical and chemical properties of 2D arsenene and arsenic, including the crystal phase and structures, chemical and environmental stability, and optical electrical properties, based on recent theoretical predictions and experimental works. Then, experimental methods to prepare 2D arsenene and arsenic, including epitaxial growth, mechanical exfoliation, and liquid-phase exfoliation, are introduced. Furthermore, we systematically discussed the applications of 2D arsenene and arsenic. Finally, we provide an outlook and perspective on the challenges of 2D arsenene and arsenic and a conclusion in this review.

2. Fundamental Properties of 2D Arsenene and Arsenic

Bulk arsenic has several allotropes that show contrasting crystal structures and electrical properties. When the thickness of arsenic is reduced to the 2D limit, exotic properties distinct from the properties in its bulk state are emerged. In particular, theoretical calculations have predicted that arsenic will display abnormal charge transport characteristics when the thickness is reduced to bilayers or monolayers, such as semimetal-to-semiconductor transitions and indirect to direct bandgap transformations. Moreover, 2D arsenic materials with different atomic structures (crystal phases) show great differences in their responses to ambient air conditions. In this section, we introduce the crystal structures, electrical characteristics, transport properties, and environmental stability of 2D arsenene and arsenic with different crystal phases in detail.

2.1. Allotropes and Corresponding Crystal Structures of Arsenic

Elemental arsenic has various allotropes, such as gray (gray) arsenic (rhombohedral), black arsenic (orthorhombic), and yellow arsenic (As_4, tetrahedral molecular structure).[72] In the past, black arsenic was usually referred to amorphous or vitreous arsenic. Nonetheless, with the rise in the studies of black phosphorus and orthorhombic arsenic, researchers habitually call orthorhombic arsenic as black arsenic. Gray arsenic is the most common and stable structure of arsenic. The crystal structure of gray arsenic is similar to that of graphite, which shows a layered honeycomb structure. However, as illustrated in **Figure 2**a, an individual layer of gray arsenic consists of buckled hexagonal rings formed by six arsenic atoms.[73] Each single layer of gray arsenic finally stacks into the bulk crystal in the ABC stacking mode. Gray arsenic is also named β-phase As, a rhombohedral phase with a space group of *R3m*. Typical gray arsenic shows the intrinsic properties of semimetals. Pumera and Sofer described gray arsenic as a layered structure material that is obviously distinct from common layered materials.[27] Because of the cross-layer orbitals of gray arsenic, the interlayer binding energy is much stronger than that of graphene, leading to semimetal behavior and high conductivity.[27] Due to the relatively weaker interlayer force compared with in-plane chemical bonds, gray arsenic is usually brittle and easily smashed into few-layer 2D materials via sonication or mechanical exfoliation.

Black arsenic (orthorhombic arsenic) is a metastable phase with a space group of *Bmab* and a crystal structure similar to that of black phosphorus. Black arsenic displays a layered orthorhombic structure consisting of puckered atomic layers arranged in parallel via van der Waals interactions (Figure 2b). Unlike gray arsenic, bulk black arsenic exhibits semiconductive properties and a direct bandgap of ≈0.3 eV.[74–76] In addition, black arsenic shows extreme in-plane anisotropic electronic and thermal properties.[75] To date, black arsenic is mostly available in the naturally occurring mineral arsenolamprite.[77] Artificial synthesis of orthorhombic arsenic is still challenging. Osters et al. recently concluded that artificially synthesized orthorhombic arsenic could only be stabilized by impurities, while pure orthorhombic arsenic is metastable and still needs to be synthesized in a kinetically controlled way.[78] Gao et al. predicted that black arsenic could transition into gray arsenic at a critical pressure of 3.48 GPa, and the structure was reversible after the release of pressure to ≈1–3 GPa.[75] Both gray arsenic and black arsenic possesses layered structures, thus enabling the possibility of generating ultrathin 2D flakes via exfoliation or epitaxial growth.

Another allotrope of arsenic, yellow arsenic, exists in the tetrahedral molecular form composed of four arsenic atoms (Figure 2c).[79] Yellow arsenic is very isomorphous with white phosphorus (P_4) and is thus largely unstable, tending to gradually transform into gray arsenic under ambient conditions. Unlike black arsenic or gray arsenic, yellow arsenic is an insulator and exhibits a waxy feature. Owing to its high reactivity among the allotypes of arsenic, yellow arsenic is commonly employed as an arsenic source for chemical reactions.

It is notable that there is also another fantastic form of arsenic, named amorphous arsenic or vitreous arsenic.[74,80] Amorphous arsenic with various densities ranging from 4.3

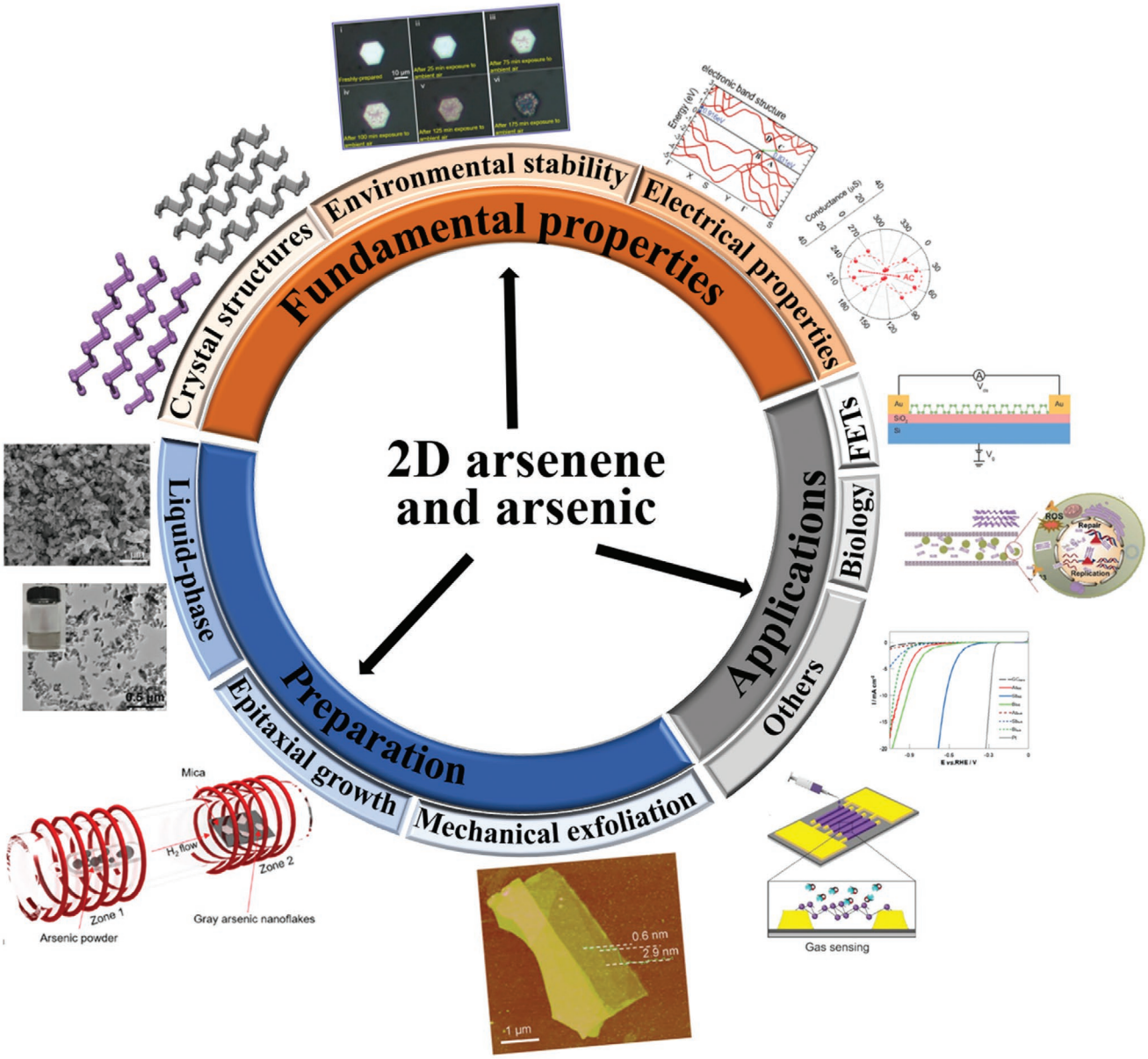

Figure 1. Schematic illustration of the fundamental properties, preparation, and applications of 2D arsenene and arsenic. Reproduced with permission.[30,38,39,43–46] Copyright 2019, American Chemical Society; Copyright 2018, WILEY-VCH Verlag GmbH & Co. KGaA, Weinheim; Copyright 2019, WILEY-VCH Verlag GmbH & Co. KGaA, Weinheim; Copyright 2017, Wiley-VCH Verlag GmbH & Co. KGaA, Weinheim; Copyright 2020, John Wiley & Sons, Inc. All rights reserved; Copyright 2015, American Physical Society.

to 5.2 g cm^{-3} can be produced, suggesting that the structure of amorphous arsenic is more open and tunable than that of the crystalline forms.[74] In addition, more than one metastable form of amorphous arsenic may exist depending on the preparation conditions.[81] Based on previous reports, the structure of vitreous-phase arsenic is similar to that of the orthorhombic phase, but some expansion and structural disorder of the interlayer and intralayer occur.[77] Furthermore, the reflection spectra of crystalline and amorphous arsenic show partial similarity, indicating their resemblance in coordination and bonding.[82] The polarization property of amorphous arsenic also indicates quasi-molecular character, and the differences between bulk and sputtered amorphous arsenic are largely ascribed to the local variations in structure with nearest neighbor layers.[81] Different optical gaps have been found in the polytropic structures of amorphous arsenic, as optical gap is highly correlated with the density of amorphous arsenic. With the decrease in the density of amorphous arsenic, the bandgap inversely increases.[74,83] Previously, thin films of amorphous arsenic were successfully prepared by electrodeposition, evaporation, and magnetron sputtering.[82] An oxygen-free amorphous arsenic film obtained by radio frequency sputtering using bulk amorphous arsenic as a target source shows an optical gap of 1.1 eV.[82] The average energy gap of

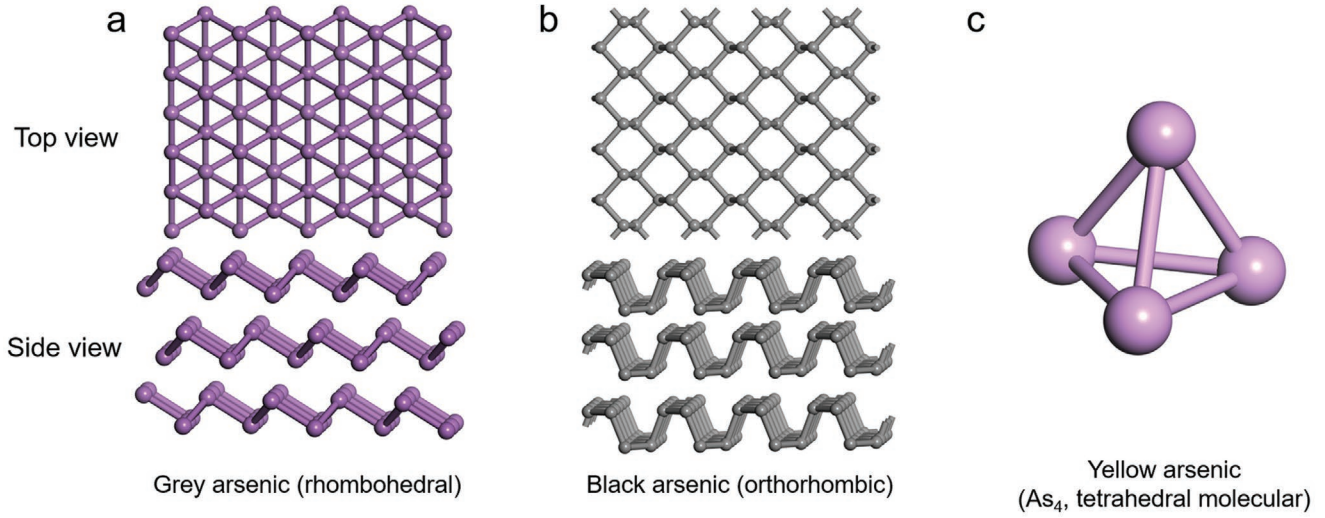

Figure 2. Atomic structures of arsenic allotropes. a) Top and side views of gray arsenic in the rhombohedral phase. b) Top and side views of the atomic structure of orthorhombic arsenic (black arsenic). c) Atomic model of yellow arsenic.

amorphous arsenic is estimated to be greater than that of gray arsenic, mainly attributed to the reduction in the strength of interlayer interactions, which strengthens the covalent bond in the amorphous structure.[82] Our recently reported works have demonstrated a wet chemistry method to convert gray arsenene into vitreous arsenene by using hydrofluoric acid aqueous solution treatment.[80] Detailed structural characterizations also confirm the typical vitrification characteristics of vitreous arsenene nanoflakes.[80] The diverse potential atomic structures of amorphous arsenic supply a wide range of possibilities for investigating and exploring the intriguing properties of 2D arsenic materials.

The crystal phase and electrical characteristics of the allotropic forms of arsenic are summarized in **Table 1**.[74] To date, the rhombohedral and orthorhombic phases of arsenic with a 2D structure have mostly been investigated and studied, and these studies depict the various intriguing chemical and physical properties of rhombohedral and orthorhombic arsenic. The layer-dependent electrical properties of gray arsenic and the anisotropy effect of black arsenic are especially prominent and have attracted great attention. In particular, many theoretical works have predicted some interesting properties of arsenic, which are waiting for verification and discovery in experiments. In addition, amorphous arsenic also has great potential to form a 2D film and may show some expected new properties.

Table 1. Crystal structures and electrical characteristics of different allotropic forms of elemental arsenic.[74]

Name	Phase	Density [g cm^{-3}]	Electronic properties
Gray arsenic	Rhombohedral	5.72	Semimetal
Black arsenic	Orthorhombic	5.54	Semiconductor (0.3 eV)
Yellow arsenic	Tetrahedral	4.3–5.2	Insulator
Vitreous arsenic	Amorphous	2.07	Semiconductor (1.2 eV)

2.2. Physical, Electrical, and Optical Properties of 2D Arsenene and Arsenic

Studies on the electrical properties of 2D arsenic and arsenene began with theoretical works in 2015. Kamal et al. and Zhang et al. investigated the kinetic stability and electronic structures of buckled and puckered honeycomb arsenic systems through first-principles calculations.[45,47,48] Buckled honeycomb arsenic is derived from gray arsenic and shares a similar honeycomb lattice with graphene while adopting buckled structures to enhance kinetic stability. Zhang et al. found that no soft phonon modes are available in the computed phonon dispersion spectra of monolayer gray arsenene, confirming its good kinetic stability (**Figure 3**a).[47] Bulk gray arsenic is a semimetal, and its semimetallic character is preserved even when the thickness is reduced to a trilayer (Figure 3b). However, a typical semimetal-to-semiconductor transition is observed when the thickness is reduced to a monolayer or bilayer, showing indirect bandgaps of 2.49 and 0.37 eV, respectively (Figure 3b). Kamal et al. investigated the stability and electronic properties of arsenene, including buckled, puckered, and planar arsenene, in detail through density functional theory (DFT).[45] They found by studying the phonon spectrum and cohesive energy that buckled and puckered monolayer arsenene is kinetically stable (Figure 3c). Then, they demonstrated that puckered monolayer arsenene is a semiconductor with an indirect bandgap of 0.831 eV (Figure 3d). Moreover, Kamal et al. and Zhang et al. discovered that it is possible to transform the bandgap of arsenene from indirect to direct via external strain or electric field application.[45,48] Zhang et al. predicted that multilayer black arsenene exhibits an intrinsic direct bandgap of ≈1 eV and has carrier mobilities as high as several thousand cm^2 V^{-1} S^{-1}.[84] Zhang et al. systematically investigated the thermodynamic stability, carrier mobilities, and band structures of nine monolayer arsenene allotropes. Among those arsenene allotropes, buckled arsenene is the most stable structure. In addition, they also confirmed the

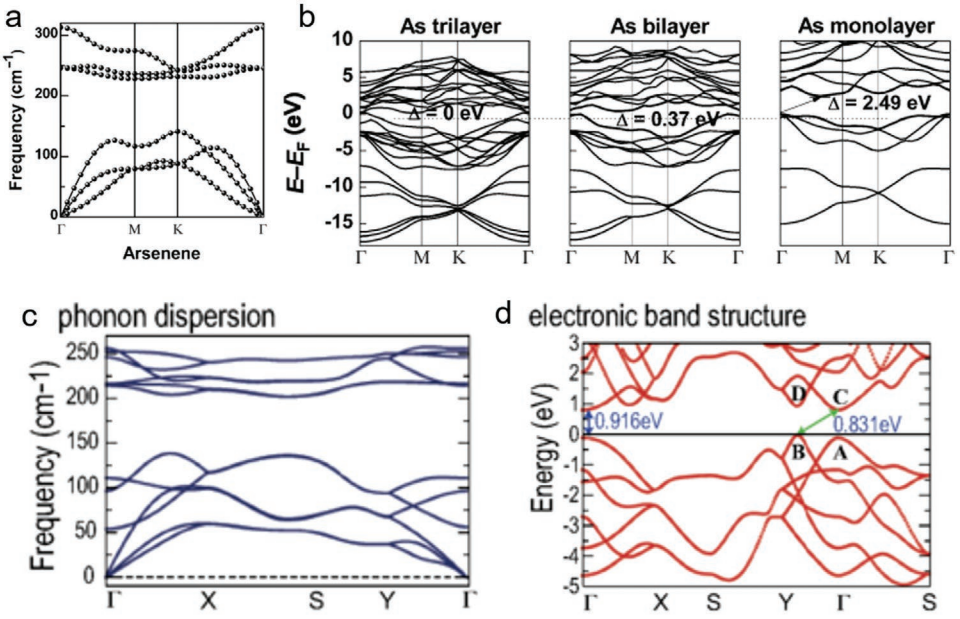

Figure 3. a) Phonon band dispersion of buckled arsenene. b) Electronic band structures of monolayer, bilayer, and trilayer of buckled arsenene. a,b) Reproduced with permission.[48] Copyright 2015, WILEY-VCH Verlag GmbH & Co. KGaA, Weinheim. c) Phonon dispersion diagram of puckered arsenene. d) Electronic band structure of puckered arsenene. c,d) Reproduced with permission.[45] Copyright 2015, American Physical Society.

broad bandgaps and superior carrier mobilities of buckled and puckered arsenene.[47]

Corresponding experimental investigations of the electrical properties of gray and black 2D arsenene and arsenic were also performed by fabricating micro/nanodevices.[30,38] The 2D gray arsenic nanoflakes typically showed thickness-dependent electrical resistance (**Figure 4**a).[30] The 10 nm thick gray arsenic nanoflake exhibited an electrical conductivity of $\approx 3.5 \times 10^3$ S m^{-1}, indicating its great potential to act as contact electrodes that are suitable for achieving good band alignments in device fabrication.[30] In contrast, 2D black arsenic nanoflake-based back-gated FETs exhibit obvious p-type behavior, showing a carrier mobility of ≈51 cm^2 V^{-1} s^{-1} and a current on/off ratio of 10^5 when V_{ds} is −1 V (Figure 4b,c).[38]

The optical properties of arsenene were also extensively studied. Kecik et al. investigated the optical properties of single- or bilayer buckled and puckered arsenene via DFT and many-body perturbation theory.[85] Single-layer arsenene shows a prominent optical response over the solar regime (within the visible and ultraviolet (UV) light ranges). Moreover, the optical properties of layered arsenene can be adjusted by both thickness and tensile strain. Vishnoi et al. then experimentally investigated the optical properties of liquid-exfoliated arsenene nanosheets and nanodots.[86] The arsenene nanosheets exhibit a bandgap of ≈2.3 eV, and the nanodots show blue PL in the range of 400–460 nm (Figure 4d,e).[86] Tsai et al. performed PL measurements for multilayer arsenene nanoribbons and estimated a bandgap of ≈2.3 eV, implying the great potential of applying multilayer arsenene in photodetectors and light-emitting devices.[58]

In addition to the semiconductive and optical properties, many works have also used theoretical calculations and experiments to observe some exotic properties of arsenene, such as QSH effects, magneto transport properties, and anisotropic thermal conductivity.[51,53,87–89] Wang et al. found that a nontrivial topological state of arsenene emerged when the applied tensile strain was larger than 11.14%.[53] A single pair of topologically protected helical edge states was observed at the edge of arsenene.[53] Then, by changing the stacking order, Zhao et al. discovered that Rashba spin splitting (RSS) and nontrivial topological electronic states can be simultaneously achieved in bilayer fluorinated arsenene (AsF).[51] The AA-stacked AsF bilayer shows an intrinsic RSS of 25 meV, which can also be tuned by biaxial strain.[51] However, the AB-stacked AsF bilayer exhibits a 2D topological insulator feature and a bulk bandgap of 140 meV due to spin–orbit coupling during $p_{x,y}$–p_z band inversion.[51] Zhang et al. experimentally observed a pair of spin-polarized surface bands on the (111) face of gray arsenic via angle-resolved photoemission spectroscopy (ARPES).[88] The state of the pair on the occupied side is similar to the typical nearly free-electron Shockley state, which is observed on noble-metal surfaces.[88] In addition, Zeraati et al. also predicted the highly anisotropic thermal conductivity of puckered arsenene along the zigzag and armchair directions using ab initio calculations.[89] Chen et al. investigated the in-plane anisotropy of a few layers of black arsenic (Figure 4f).[46] The structure, conductance, and thermal conductivity of black arsenic along the armchair (AC) and zigzag (ZZ) directions are systematically studied, showing the highest mobility ratio among the known 2D crystals.[46] In particular, Zhao et al. found an extremely large magnetoresistance of up to 15 000 000% in a gray arsenic crystal at 1.8 K under a magnetic field of 9 T.[87] Moreover, electron energy loss spectroscopy showed that black arsenic nanoflakes demonstrated a thickness-dependent dielectric response.[65]

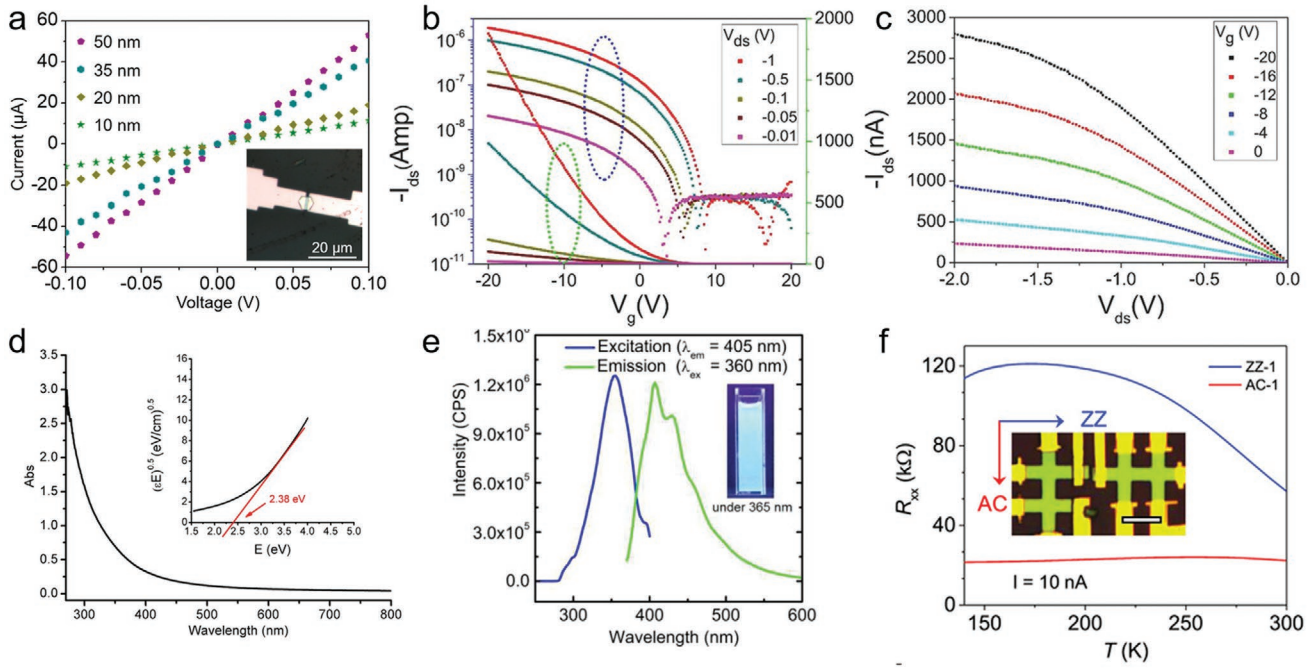

Figure 4. a) *I–V* curves of freshly prepared gray arsenic nanoflakes with different thicknesses. Reproduced with permission.[30] Copyright 2019, American Chemical Society. b,c) Output and transfer characteristics of monolayer black arsenic. Reproduced with permission.[38] Copyright 2018, WILEY-VCH Verlag GmbH & Co. KGaA, Weinheim. d) Absorption spectrum of arsenene nanosheets. e) Emission and excitation spectra of arsenic nanodots synthesized by sonication in toluene. d,e) Reproduced with permission.[86] Copyright 2018, Royal Society of Chemistry. f) Temperature-dependent resistance of black arsenic along the AC and ZZ directions. Reproduced with permission.[46] Copyright 2018, WILEY-VCH Verlag GmbH & Co. KGaA, Weinheim.

2.3. Chemical and Environmental Stability of 2D Arsenene and Arsenic

Similar to black phosphorus, arsenic crystals are sensitive to humidity and air, resulting in a black oxidation layer on their surface. In addition, the ambient air instability is normally enhanced when the arsenic crystal becomes 2D. Our previous work primarily investigated the environmental stability of 2D gray arsenic nanoflakes using optical microscopy and Raman spectroscopy.[30] As illustrated in **Figure 5**a,b, the hexagonal gray arsenic nanoflake shows obvious degradation after ambient air exposure at room temperature. In particular, chemical degradation tends to begin at edge sites and some center spots. With the continuous exposure of ambient air, degradation will finally spread into the total nanoflake, and the surface of the nanoflake turns deep yellow and dark brown. The corresponding Raman spectrum of ambient air-exposed gray arsenic nanoflakes shows a broad band and two more Raman peaks than that of freshly prepared arsenic nanoflakes, indicating that gray arsenic nanoflakes will undergo chemical degradation after exposure to ambient conditions and transform into amorphous arsenic and As_2O_3.[30]

Black arsenic also undergoes considerable structural destruction in several days, but its rate of degradation is relatively slow compared with that of gray arsenic, which occurs in a few hours.[65] In particular, black arsenic shows a loss of arsenic elements and no accumulation of arsenic oxide after ambient air exposure (Figure 5c). Yun et al. emphasized the effect of humidity on black arsenic nanoflakes, speculating that volatile products formed through the interaction between arsenic and water vapor in air.[65] **Figure 6**a,b compares the compositions of black arsenic flakes stored in humid air, dry air, and dry vacuum to investigate degradation in detail. The degradation of most regions of black arsenic flakes occurred in just 2 days, while no obvious degradation was observed in dry air (humidity of ≈2.5%). The chemical composition of the humid air-conditioned black arsenic flake also demonstrates a fast increase in the oxygen percentage, while the increase in the oxygen percentage is relatively slow for the dry air-conditioned black arsenic flake. Systematic studies on the stability of black arsenic confirmed that oxygen alone in air does not react with black arsenic and highlighted the high sensitivity of black arsenic toward steam in air.[65]

The ambient air exposure of arsenic nanoflakes will seriously destroy their crystal structure and change their chemical composition, even though black arsenic (several days) is more stable than gray arsenic (several hours). The unstable feature of arsenic nanoflakes in ambient air will greatly impede sample preservation and characterization. In particular, for the practical application of electronic transistors based on arsenic nanoflakes, devices must be quite resistant to environmental conditions. Thus, several strategies have been developed to passivate and protect arsenic nanoflakes from ambient air, such as interfacial interactions or isolation from humidity. Our previous work demonstrated a universal method to passivate gray arsenic nanoflakes and estimated the antidegradation efficiency of polymer-passivated gray arsenic nanoflakes.[30] We demonstrated that some functional polymers can effectively suppress the degradation of gray arsenic nanoflakes in ambient air for at least 50 days (Figure 6a). In addition, the effective protection

time of polymer-coated gray arsenic nanoflakes is obviously related to the interfacial interaction between the polymer and arsenene, which is helpful for estimating the antidegradation efficiency of polymer-passivated gray arsenic nanoflakes and screening polymers with high antidegradation efficiencies.[30] Importantly, the gray arsenic nanoflakes show almost identical optical contrast and Raman spectra before and after the removal of polyethylene glycol (PEG). The polymer passivation strategy greatly improves the convenience of preserving and transferring gray arsenic nanoflakes in an atmospheric environment, facilitating further device fabrication and sample characterization.

Black arsenic nanoflakes are especially sensitive to humidity in the air. Preventing contact between water vapor and arsenic seems to be an effective way to protect arsenic nanoflakes. Yun et al. demonstrated that dry air and dry vacuum are both helpful for protecting black arsenic nanoflakes (Figure 6b).[65] The dry vacuum-conditioned black arsenic flakes degraded in the same way as they degraded in ambient air but with a minor amount and slow speed. The dry air-stored samples showed no obvious visible degradation, even after a month, indicating the formation of a protective layer on black arsenic nanoflakes. They suggested that the thin arsenic oxide layer generated on the surface of black arsenic nanoflakes in dry air may hinder further nondirectional degradation. In contrast, the arsenic nanoflakes prepared via liquid-phase exfoliation showed relatively good stability while stored in solvents. The gray arsenic nanoflakes prepared by sonicating in dimethylsulfoxide (DMSO) show unchanged Raman spectra after storage in DMSO for 10 days (Figure 6c).[39] The gray arsenic nanoflakes produced in chloroform first depicted fast sedimentation, then stabilized in ≈24 hours, and finally showed unchanged absorbance over time (Figure 6d).[59] The relatively high stability may be attributed to surface functionalization during the ultrasonic process and solvent storage, which isolated the arsenic nanoflakes from moisture and oxygen in ambient air.

The exposure of arsenic nanoflakes to ambient air will have a significant influence on their intrinsic electrical and optical properties. Zhong et al. investigated the ambient stability of black arsenic nanoflake FETs in detail.[38] They found that the few-layer black arsenic transistor still maintains good Ohmic contact after 26 days of ambient air exposure.[38] However, the carrier mobility decreased from the initial value of 26 to

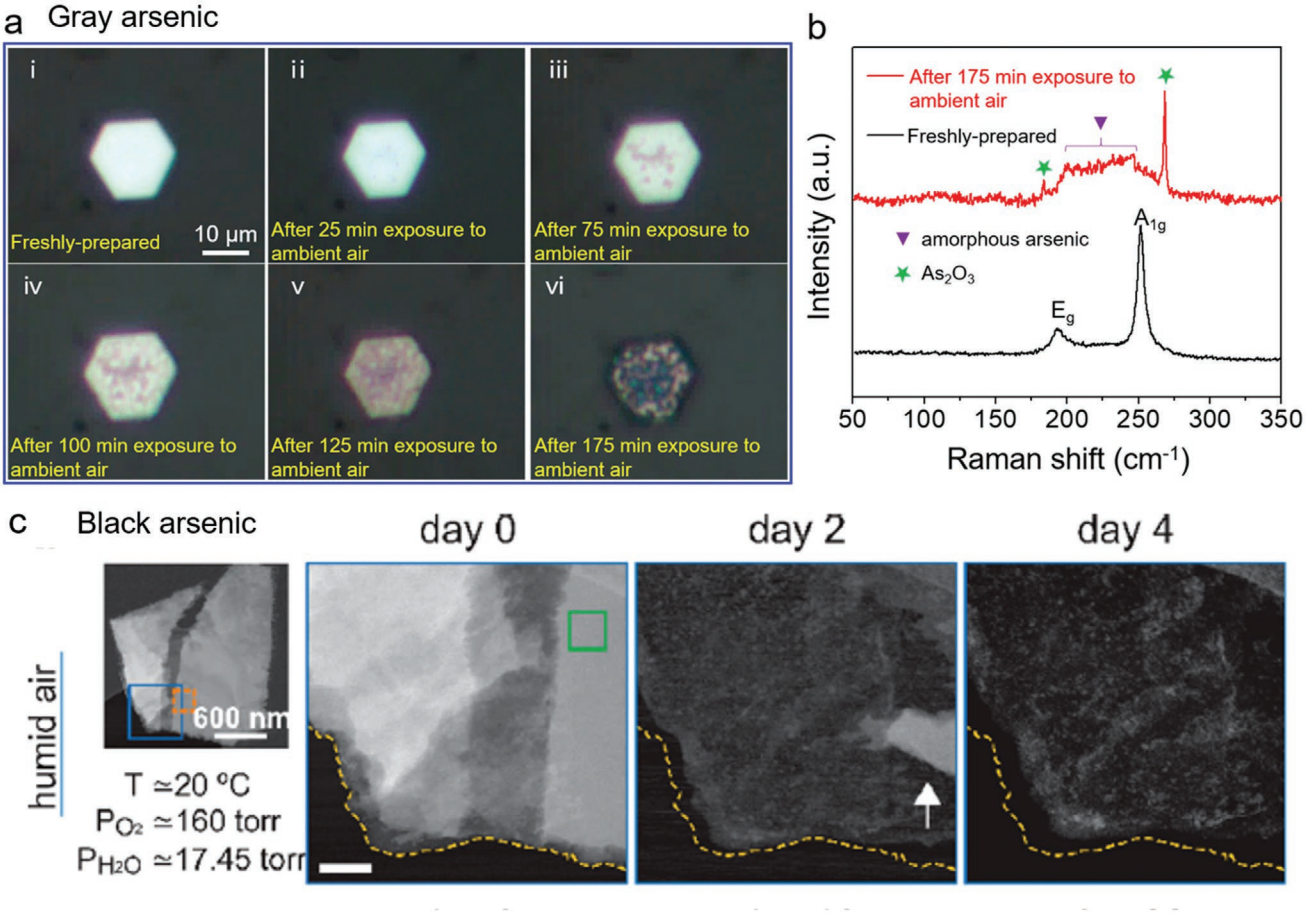

Figure 5. a) Optical images of a gray arsenic nanoflake with different periods of ambient air exposure. b) Corresponding Raman spectra of the freshly prepared gray arsenic nanoflake and the gray arsenic nanoflake after 175 min of ambient air exposure. a,b) Reproduced with permission.[30] Copyright 2019, American Chemical Society. c) High-angle annular dark-field scanning transmission electron microscopy (HAADF-STEM) images of black arsenic nanoflakes with different degradation times. Reproduced with permission.[65] Copyright 2020, American Chemical Society.

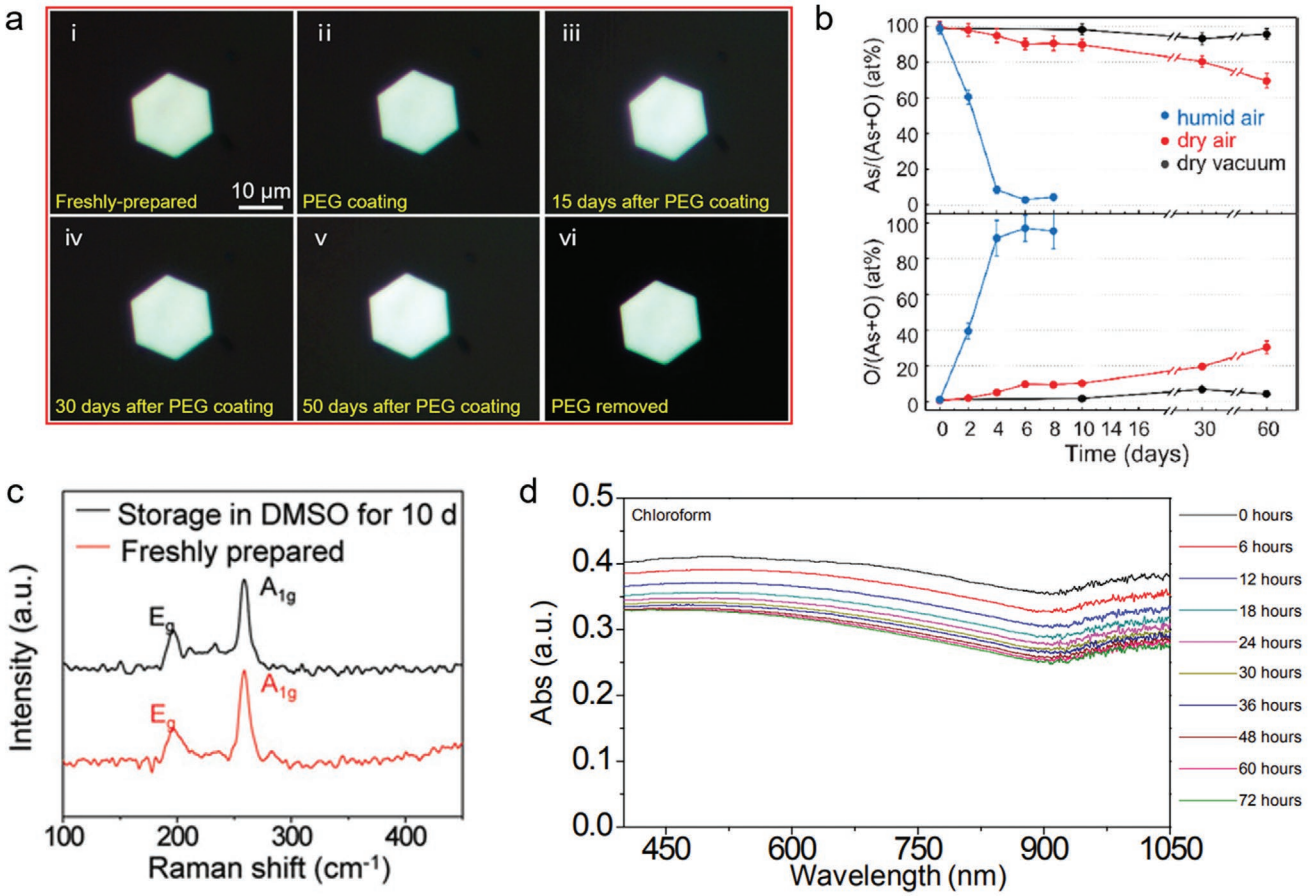

Figure 6. a) A gray arsenic nanoflake in the freshly prepared state, after PEG coating and after PEG removal. Reproduced with permission.[30] Copyright 2019, American Chemical Society. b) Relative elemental composition evolution of black arsenic flakes over time. Reproduced with permission.[65] Copyright 2020, American Chemical Society. c) Raman spectra of freshly prepared gray arsenic nanoflakes after 10 days of storage in DMSO. Reproduced with permission.[39] Copyright 2020, John Wiley & Sons, Inc. d) Absorption spectrum of freshly prepared arsenic nanoflakes stored in chloroform as a function of time. Reproduced with permission.[59] Copyright 2019, Royal Society of Chemistry.

≈8.4 cm^2 V^{-1} s^{-1}, showing ≈67% decay (**Figure 7**a). As the rate of the decrease in current in the OFF state is larger than that in the ON state current, the on/off ratios showed the opposite behavior as carrier mobility during ambient air exposure, suggesting an ≈40% increase from 69 to 97 (Figure 7a). They claimed that the evolution of the electrical properties of black arsenic is mainly caused by oxidation during ambient air exposure (Figure 7b). The air stability of black arsenic is obviously superior to that of black phosphorus.[38,90] Our previous work has also studied the electrical conductivity of gray arsenic nanoflakes as a function of ambient air exposure duration.[30] The electrical conductivity of a 50 nm thick gray arsenic nanoflake dramatically decreases in ≈200 min when exposed to an air environment, indicating that the gray arsenic nanoflakes are more sensitive to ambient air than black arsenic (Figure 7c). However, the PEG-passivated gray arsenic nanoflake maintained a current with an order of magnitude equivalent to that of the initial current after storage in ambient air for 50 days, suggesting only a slight decay in electrical conductivity and weak destruction of crystal quality. Moreover, the transfer curve of the gray arsenic nanoflake-based device after 250 min in ambient air showed a decrease in drain currents with respect to gate voltage and exhibited a p-type feature (Figure 7d). This phenomenon supplies the possibility of manipulating the electrical properties of gray arsenic nanoflakes by controlling the degree of oxidation.

The excellent physical, electrical, and optical properties of 2D arsenene and arsenic investigated by theoretical calculations and experiments imply their great potential and broad applications in spintronics, magnetic sensors, photovoltaic devices, and optoelectronic devices. Moreover, the theoretically calculated kinetic stability of arsenene also reveals the probability of the experimental preparation and development of single-layer arsenene samples.

3. Preparation of 2D Arsenene and Arsenic

The experimental realization of 2D arsenene and arsenic is of key importance to discovering and verifying their tremendous properties and applications. Encouragingly, the preparation and realization of 2D arsenene and arsenic have been carried out successfully in recent years. The methods include epitaxial growth, mechanical exfoliation, and liquid-phase exfoliation,

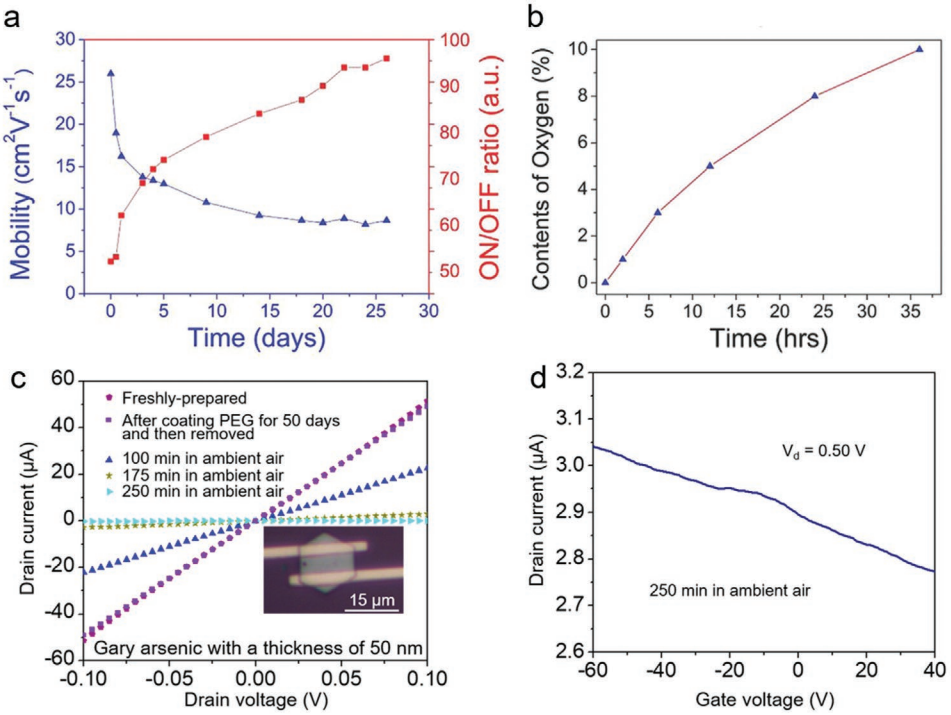

Figure 7. a) Carrier mobilities and on/off ratios of a black arsenic transistor as a function of ambient air exposure time. b) The oxygen percentage in black arsenic with different durations of ambient air exposure. a,b) Reproduced with permission.[39] Copyright 2020, John Wiley & Sons, Inc. c) *I–V* curves of a gray arsenic nanoflake-based device in the freshly prepared state, with different durations of ambient exposure and with PEG passivation. d) Transfer characteristic curve of a gray arsenic nanoflake-based device after 250 min of ambient air exposure. c,d) Reproduced with permission.[30] Copyright 2019, American Chemical Society.

which have respective advantages and disadvantages. For example, mechanical exfoliation is an effective way to obtain high-quality crystals with low yields and highly random samples. In contrast, liquid-phase exfoliation can be used to prepare 2D arsenene and arsenic in large quantities, but the amounts of defects and oxides on the samples also increase in relatively harsh preparation environments. These methods can be rationally selected based on the requirements of applications or research.

Despite "up-down" methods (such as mechanical exfoliation and liquid-phase exfoliation), "bottom-up" strategies (including molecular beam epitaxy (MBE), chemical vapor deposition (CVD), physical vapor deposition (PVD), and plasma-assisted pyrolysis growth, etc.) are also effective and crucial in preparing high-quality 2D materials toward large-scale practical device production. To grow 2D arsenene and arsenic materials on certain substrates, the selection of appropriate precursors and substrates is vital. For example, monolayer gray arsenene has been successfully grown on Ag(111) substrate via MBE by heating InAs crystal to generate As precursor species.[91] The crystallization temperature mostly dominated the synthesized crystal phase of arsenene. The crystallization temperature of arsenic crystals above 360 °C, less than 300 °C, or rapid cooling will lead to the formation of gray arsenic, amorphous arsenic, and yellow arsenic, respectively. As a typical example, our recent work have prepared single-crystal gray arsenene by controlling the crystallization temperature at 325 °C.[30] Not just arsenene, the reasonable selection of precursors and the regulation of crystallization temperature are vital for the growth of all pnictogen 2D materials. Appropriate precursors can generate pnictogen clusters which are decisive for epitaxial growth. For example, the sublimation of white phosphorus will generate P_4 molecules, which is not suitable for the growth of black phosphorus crystal. Besides, controlling the crystallization temperature can effectively promote the formation of chemical bonds with different bond energies, resulting in the formation of different crystal phases of 2D pnictogen materials.

In this section, we will summarize the recent experimental realization of 2D arsenene and arsenic and subdivide these preparation methods into three strategies: mechanical exfoliation, epitaxial growth, and liquid-phase exfoliation.

3.1. Epitaxial Growth

Epitaxial growth is also an effective way to obtain 2D materials with high crystal quality and an appreciable lateral size.[92–96] This process of precursor evaporation is followed by epitaxial growth on the substrate surface. The definition of epitaxial growth is very broad and includes MBE, CVD, PVD, and plasma-assisted pyrolysis growth. Epitaxial growth complements mechanical exfoliation, especially for materials that are very difficult to mechanically peel. Unlike mechanical exfoliation, epitaxial growth alleviates much randomness, the thickness is relatively controllable, and the film uniformity is good. By adjusting the growth parameters, such as the

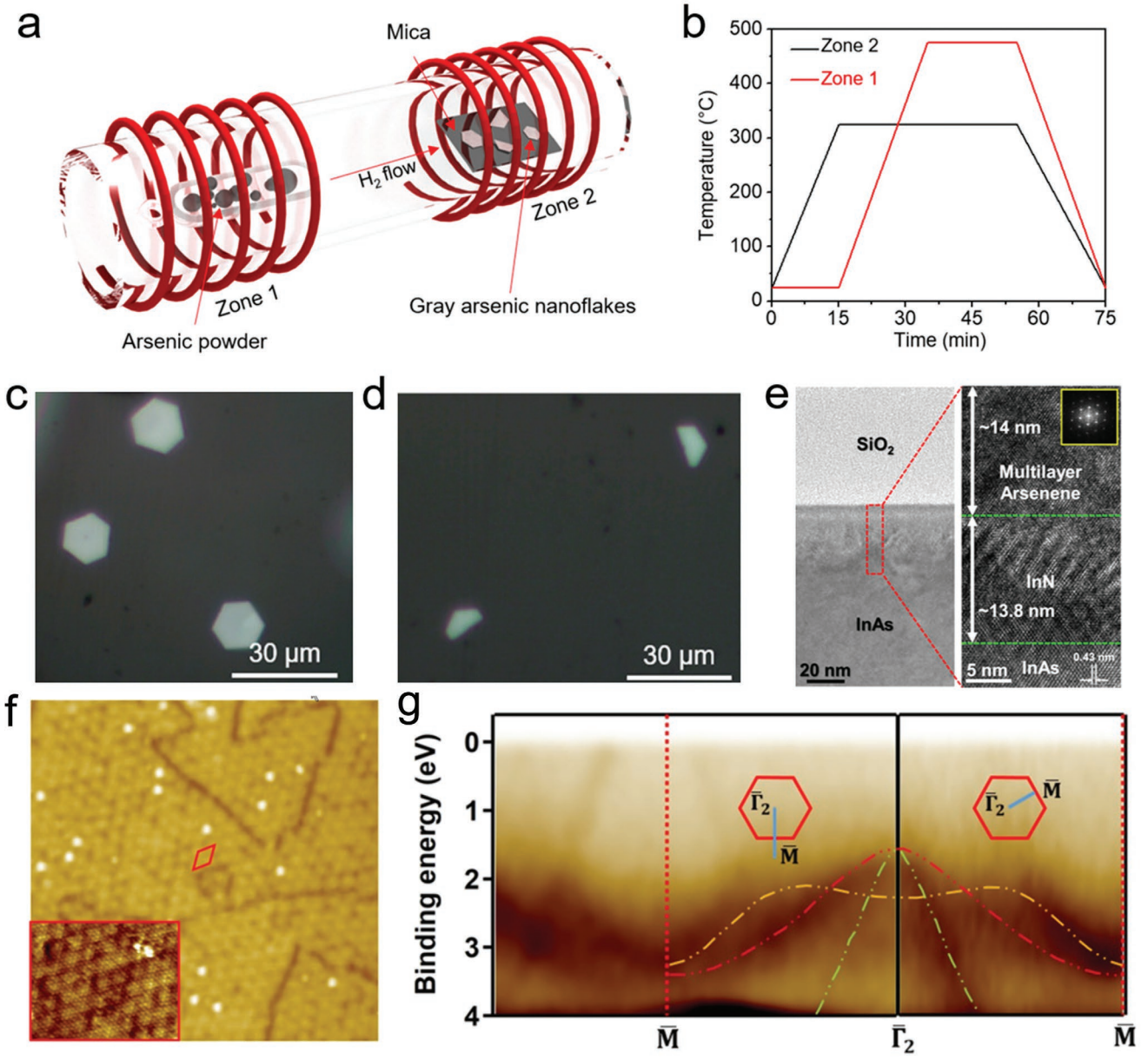

Figure 8. a) Schematic illustration of a two-zone tube furnace system. b) Temperature evolution curves of zone 1 and zone 2. c,d) Optical images of hexagonal and half-hexagonal gray arsenic nanoflakes. c,d) Reproduced with permission.[30] Copyright 2019, American Chemical Society. e) Cross-sectional TEM image of the multilayer arsenene/InN/InAs. Reproduced with permission.[58] Copyright 2016, American Chemical Society. f) STM image of arsenene layer on Ag (111) substrate. g) Band structures of arsenene investigated by experimental ARPES characterization and theoretical calculation. f,g) Reproduced with permission.[91] Copyright 2020, IOP Publishing Ltd.

temperature, air pressure, carrier gas flow, source material weight, substrate type and source–substrate distance, the layer number, lateral size, morphology, growth orientation, and defects of the 2D material can be regulated and controlled. This method has the advantages of reasonable cost, good extensibility, and strong controllability, which is of great significance for basic research and the development of 2D materials. Moreover, it is also a method with great potential for preparing large-scale single crystal or chip-level 2D materials, which is an essential requirement for the industrialization of 2D materials.

Our previous work reported the growth of hexagonal and half-hexagonal gray arsenic nanosheets on mica substrates via a van der Waals epitaxial growth method using a two-zone tube furnace system (**Figure 8**a).[30] We designed a two-zone method to sublimate the arsenic precursor and epitaxially grow arsenic nanoflakes (Figure 8a,b). By controlling the temperature of the growth zone, a phase of gray arsenic is obtained (Figure 8c,d). As-synthesized gray arsenic nanoflakes show hexagonal and half-hexagonal shapes with a diagonal length up to 20 μm. Moreover, as-synthesized gray arsenic nanoflakes exhibit a single-crystalline feature and rhombohedral phase. Tsai et al.

developed a plasma-assisted process to synthesize multilayer arsenene nanoribbons on InAs (Figure 8e).[58] Based on the plasma-assisted process, nitrogen ions introduced into InAs prefer to react with indium during the heat treatment process, and arsenic atoms are extruded to form an arsenic layer on the surface.[58] The prepared arsenene can be optimized by adjusting the annealing time, plasma power, and plasma exposure time. In particular, Shah et al. recently have presented the electronic structure of an monolayer arsenene on Ag(111) substrate in ultrahigh vacuum system.[91] By using scanning tunneling microscope (STM) and ARPES characterizations, they found that the arsenene layer shows a lattice constant of 3.6 Å and three 2D electron bands in the electrical structure below the Fermi level (Figure 8f,g).[91]

Epitaxial growth is a method with important practical significance. In particular, the merits of high crystal quality and large-scale preparation are of great significance for the fabrication of devices at the industrial level. Simultaneously, difficulties, such as an uncontrolled growth environment and complex growth parameters, also need to be overcome.

3.2. Mechanical Exfoliation

The typical mechanical exfoliation method uses "Scotch tape" to obtain a few layers of 2D materials.[97–99] In this process, the surface of the bulk materials contacts the tape and is then removed from the bulk materials. The material attached to the tape can be reattached with new tape to make it thinner. When the 2D material is thin enough, the tape with 2D materials can adhere to a clean substrate surface. Due to van der Waals forces, the few-layer 2D materials will stay on the substrate when the Scotch tape is removed from the substrate. If this process is repeated enough times, 2D materials will become thinner until a single layer is formed.

The mechanical exfoliation of arsenic crystals occurs mainly in the black arsenic phase.[38,46,65] Black arsenic has a weaker interlayer force, which is more conducive to achieving a thin arsenic layer. Chen et al. first prepared 2D black arsenic by mechanically exfoliating natural minerals.[46] **Figure 9**a shows a typical atomic force microscopy (AFM) image of a thin black arsenic nanoflake with a step size of 0.6 nm. Subsequently, Zhong et al. successfully exfoliated monolayer black arsenic flakes with a thickness of 0.7 nm from bulk natural minerals onto Si/SiO_2 (300 nm) substrates (Figure 9b).[38] Moreover, Yun et al. purchased commercial black arsenic crystals prepared by a chemical vapor transport technique using arsenic as a precursor from 2D Semiconductors Inc.[65] Then, 2D black arsenic nanoflakes were also successfully exfoliated from bulk black arsenic crystals using Scotch tape (Figure 9c).[65]

The mechanical exfoliation method can produce 2D black arsenic with high crystal quality, and the process is relatively low cost, convenient, and without chemical contamination. It is a credible and effective tool for studying the basic physical, optical, and electrical properties of novel 2D black arsenic, accelerating the development of 2D black arsenic. However, its yield is relatively low, and the ability to control layer thickness, shape, and lateral size is limited. Therefore, it is not suitable for the mass production of 2D materials with controllable thickness and lateral size. In particular, for layered materials with strong interlayer forces, such as gray arsenic or bismuth, it is relatively difficult to directly obtain a single- or few-layer film. In addition, the low yield of 2D black arsenic obtained by mechanical exfoliation restricts some of its applications.

3.3. Liquid-Phase Exfoliation

As an alternative method, liquid-phase exfoliation is a high yield and reliable method for the mass production of 2D materials.[100–103] The primary characteristic of liquid-phase exfoliation is the applied external force, which induces the breaking of the interlayer force.[104] In addition, with the help of an intercalator agent, such as positive ions, molecules, or radicals, the interlayer distance is expanded, making the exfoliation of 2D materials via external sonication easier and larger scale. According to the exfoliation principles, exfoliation can be divided into sonication-assisted exfoliation,[101,103] mechanical

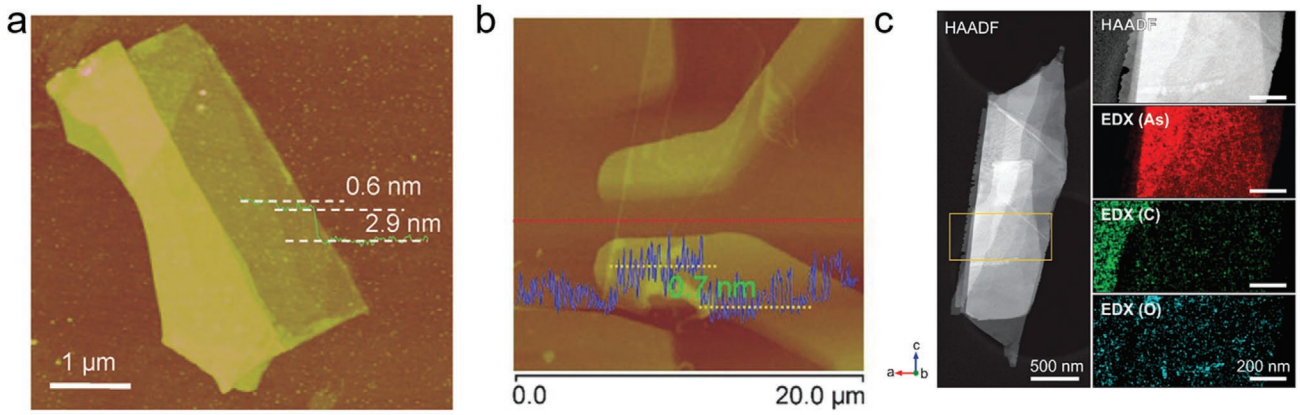

Figure 9. a) Mechanically exfoliated black arsenic with a single layer step. Reproduced with permission.[46] Copyright 2018, WILEY-VCH Verlag GmbH & Co. KGaA, Weinheim. b) Single-layer black arsenic exfoliated from natural minerals. Reproduced with permission.[38] Copyright 2018, WILEY-VCH Verlag GmbH & Co. KGaA, Weinheim. c) HAADF-STEM image and corresponding ESX elemental maps of a black arsenic nanoflake prepared by mechanical exfoliation. Reproduced with permission.[65] Copyright 2020, American Chemical Society.

force-assisted exfoliation,[44] insertion-assisted expansion exfoliation,[105–107] and guest ion- or molecular in-layer material-assisted exfoliation.[108,109] Liquid-phase exfoliation can be used to prepare a large yield of 2D materials, which are very suitable for applications in catalysis, energy storage, and other fields.[110–113] Next, we introduce recent work on the liquid-phase exfoliation of arsenic with different exfoliation mechanisms.

Sonication-assisted liquid-phase exfoliation is one of the most convenient ways to prepare 2D materials. The cavitation bubbles generated by ultrasonic waves break up the layered crystals and produce 2D nanosheets.[100] Normally, the surface free energy match between solvents and layered crystals is necessary to minimize the energy cost and reaggregation during exfoliation.[114,115] In addition, using organic solvents with higher boiling points and surface tension usually produces 2D materials with a higher exfoliation efficiency.[116] Vishnoi et al. isolated few-layer arsenene from bulk gray arsenic crystals via sonication in polar solvents of *N*-methyl-2-pyrrolidone (NMP).[86] Moreover, arsenene sheets can be functionalized with 4-nitrobenzenediazonium salts.[86] However, by changing the solvents to an nonpolar toluene solvent, arsenene nanodots were achieved.[86] Our previous work also reported the direct exfoliation of gray arsenic crystals by sonicating in DMSO.[39] DMSO was selected as the sonication solvent due to its relatively high polarity, thermal stability, and water miscibility, which are convenient for sample preparation and biological injection into cells. The prepared arsenene nanosheets show the typical morphology of nanoflakes, with a median size of 200.8 nm and ultrathin features (**Figure 10**a–c), confirming the successful exfoliation of gray arsenic crystals into arsenene nanosheets.[39]

Beladi-Mousavi et al. systemically investigated the influence of solvents on the productivity of 2D gray arsenic.[43] They used different organic solvents, such as hexane, isopropyl alcohol (IPA), acetone, methanol, DMSO, NMP, and water, to produce 2D gray arsenic and screen the optimal solvent.[43] The resulting arsenene nanosheet dispersions all showed brown or gray colors (Figure 10d). The hexane and NMP dispersions illustrated the lightest and darkest colors, respectively (Figure 10d). Then, the concentration of the as-prepared arsenene nanosheet dispersions was plotted as a function of the boiling point (Figure 10e) and surface tension (Figure 10f) of the solvents. Solvents with a higher boiling point and surface tension usually produced the highest concentrations of gray arsenene nanosheets.[43] Despite the surface tension and polarity, our previous work has also found that the interaction between monolayer arsenene and solvents is also correlated with the yields of arsenene nanosheets prepared by liquid-phase exfoliation.[59] We calculated the adsorption energy and charge transfer between monolayer arsenene and 14 kinds of solvents. Then, three representative aprotic solvents (cyclohexane, tetrahydrofuran, and chloroform) were chosen to exfoliate bulk arsenic crystals into arsenene nanosheets, showing a positive correlation between interaction and yields (Figure 10g–i).

In addition to ultrasonic waves, externally imposed shear force was also reported as an effective way to break the interlayer interaction of gray arsenic. Pumera et al. used the aqueous shear exfoliation method to obtain As, Sb, and Bi nanosheets.[23,44,117] In their project, a kitchen blender was used to exfoliate and disperse pnictogen (As, Sb, Bi) nanosheets, and sodium cholate was used as an aqueous surfactant (**Figure 11**a). The characterizations of the prepared arsenene nanosheets showed a decrease in thickness, sheet-to-nanosheet scale, and partial oxidation (Figure 11b).[23] In addition, the exfoliated arsenene nanosheets can be covalently modified with chlorocarbene generated from dichloromethane and butyllithium, which leads to the introduction of chloromethylene groups.[63] On the basis of shear exfoliation, Antonatos et al. changed the solvent to deoxygenated acetonitrile, which is a low-boiling point solvent that can maintain a stable dispersion of 2D materials, can prevent the degradation of 2D materials from oxidation, and is easy to remove.[62] After the high-energy shear force exfoliation process, high yields and stable colloidal solutions of gray and black arsenene nanosheets were achieved. Sturala et al. introduced a photo-assisted method using UV light irradiation and chromium hexacarbonyl to covalently functionalize and exfoliate gray arsenic crystals simultaneously.[64]

Insertion-assisted expansion exfoliation combined with sonication-assisted exfoliation is another effective method used for the large-scale production of thin 2D materials. The electrochemical exfoliation strategy normally employs the intercalation of diverse cations into bulk layered materials in nonaqueous electrolytes under the drive of electrodynamic potential.[106,118] Kovalska et al. successfully exfoliated native arsenic (black arsenic) via a low-potential electrochemical exfoliation strategy in *N*,*N*-dimethylformamide solvents using ammonium hexafluorophosphate (NH_4PF_6) as active ions.[61] The low-potential electrochemical exfoliation process, in short, included three steps: wetting, accumulation, and intercalation (Figure 11c).[61] The "wetting" step occurred by applying a bias of −1 V for 2 min to black arsenic. Then, by increasing the voltage to −2.5 V and sustaining it for 30 min, NH_4PF_6 molecules accumulated against the anode. Finally, a low voltage of −3.8 V was used to drive the "intercalation" of NH_4^+ ions into the interlayer of black arsenic crystals, leading to the exfoliation and dissociation of a few layers of gray arsenene. The products showed a net-like porous shape composed of 2D flakes with a thickness of ≈0.6 nm and a lateral area of ≈1.5 µm (Figure 11d,e).[61]

Liquid-phase exfoliation is an effective way to achieve 2D arsenene nanosheets with high yields at the milligram level and relatively good crystal qualities, which is very compatible for applications that require a large number of samples, such as energy storage, multifunctional composites, printing inks, and photo- and electro catalysis. However, due to the adsorption of the solvent molecule, high-energy process, and ion interaction, the performances of electronic devices fabricated by 2D arsenic obtained via liquid-phase exfoliation are generally inferior to those obtained by mechanical exfoliation or epitaxy growth. Overall, the weaknesses and advantages of those methods are complementary for the development and progress of 2D arsenene and arsenic.

4. Applications of 2D Arsenene and Arsenic

With the successful preparation of 2D arsenene and arsenic, their potential applications are continuously identified and developed. Because of the multiple allotropes and crystal

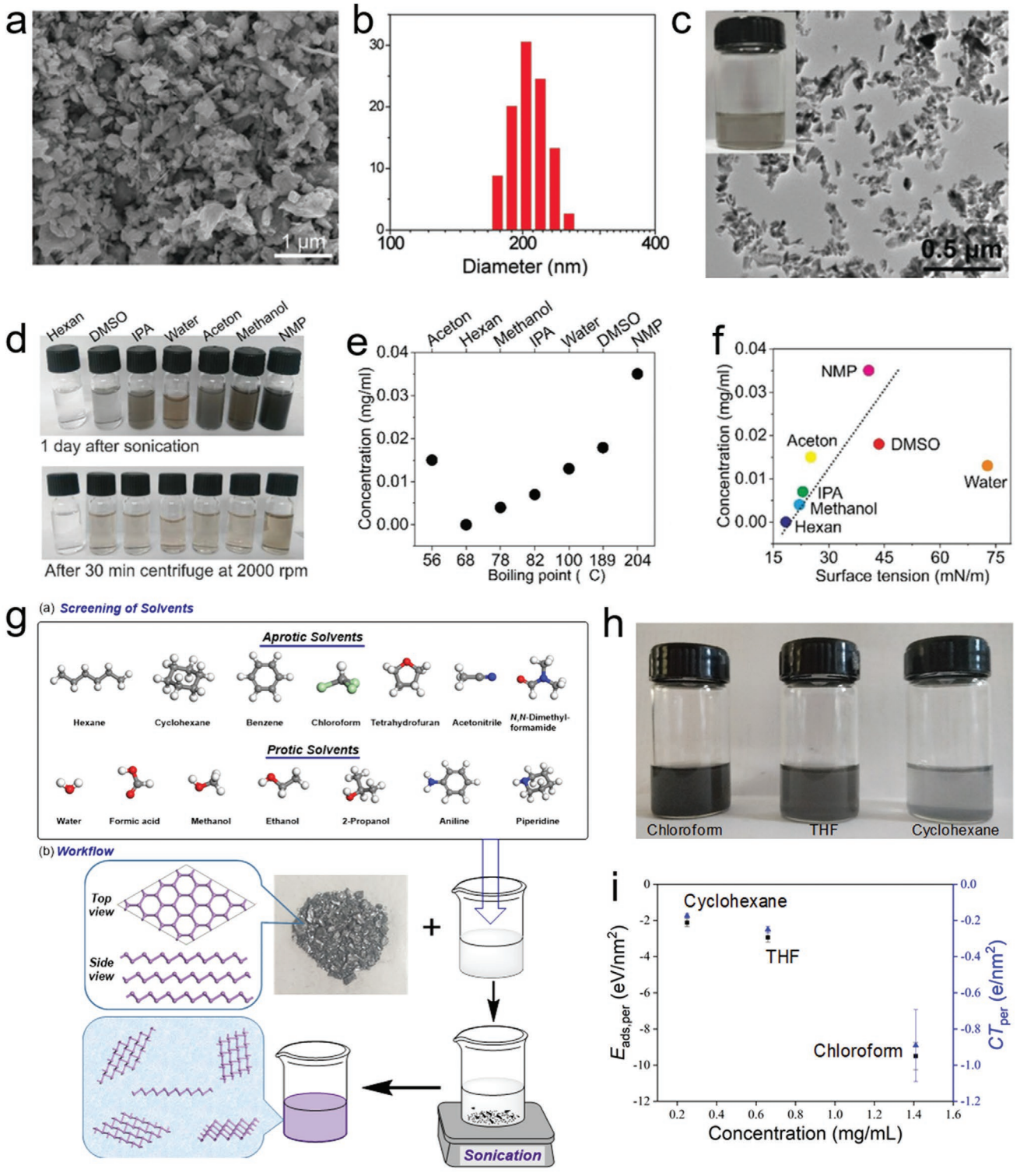

Figure 10. a) SEM image of arsenene nanosheets prepared by sonicating in DMSO. b) The size distribution of the arsenene nanosheets. c) Corresponding TEM image of as-prepared arsenene nanosheets; the inset illustrates a digital photo of arsenene nanosheets dispersed in DMSO. a–c) Reproduced with permission.[39] Copyright 2020, John Wiley & Sons, Inc. All rights reserved. d) Digital photo of arsenene nanosheets dispersed in various solvents for 1 day after ultrasonication (upon) and after centrifugation at 2000 rpm (below). e) The concentrations of as-prepared arsenene as a function of the boiling points of different solvents. f) The concentrations of as-prepared arsenene as a function of different solvents with different surface tensions. e,f) Reproduced with permission.[43] Copyright 2019, John Wiley & Sons, Inc. g) Schematic illustration of the screening of solvents and workflow for the liquid-phase exfoliation of gray arsenic crystals. h) Arsenene nanosheet dispersions exfoliated in chloroform, tetrahydrofuran (THF), and cyclohexane. i) Yields of arsenene nanosheets as a function of adsorption energy and charge transfer. Reproduced with permission.[59] Copyright 2019, Royal Society of Chemistry.

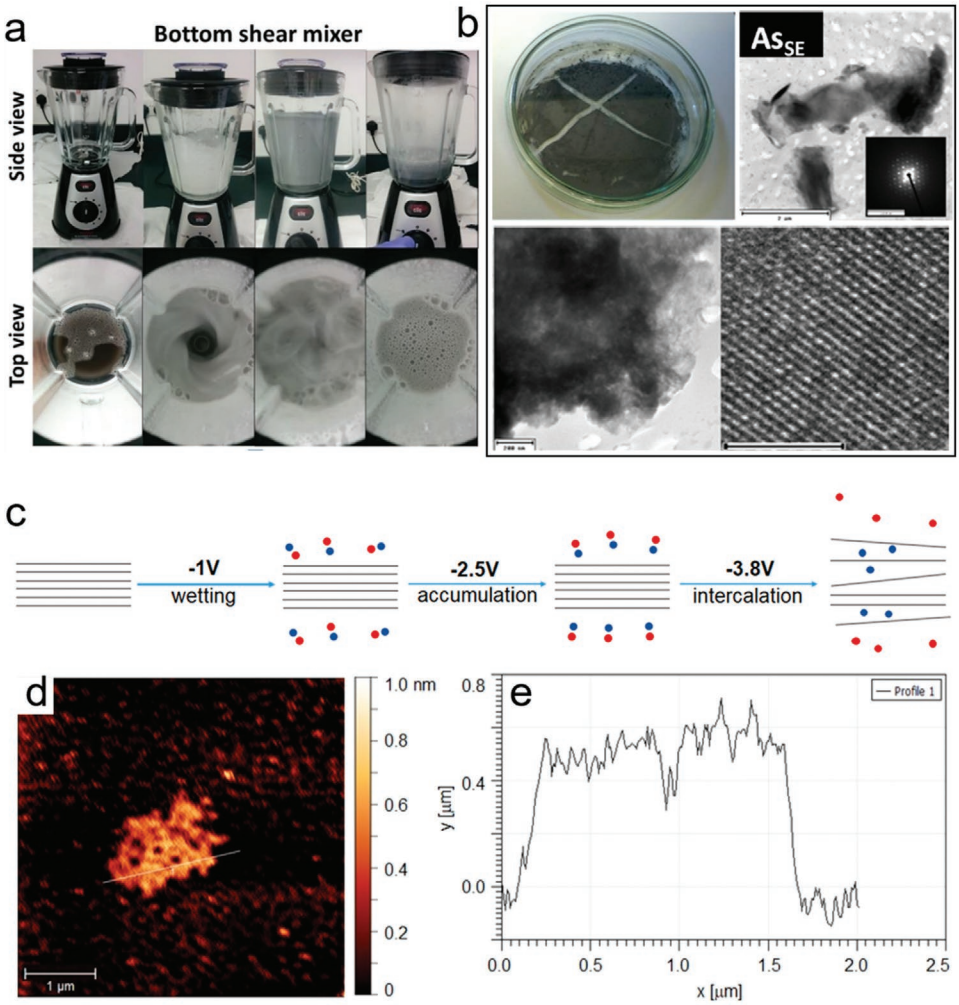

Figure 11. a) Top view and side view photographs of the kitchen blenders used for the exfoliation of pnictogens (As, Sb, and Bi) by shear force exfoliation. b) Photographs and TEM characterizations of the resulting arsenene nanosheets prepared by shear force exfoliation. a,b) Reproduced with permission.[44] Copyright 2017, John Wiley & Sons, Inc. All rights reserved. c) Schematic illustration of the low-potential electrochemical exfoliation of black arsenic. d,e) AFM image and corresponding height profile of net-like porous-shaped 2D arsenene nanosheets. c–e) Reproduced with permission.[61] Copyright 2020, American Chemical Society.

phases of arsenic, 2D arsenene and arsenic have diverse properties and features, enabling a wide range of 2D arsenene and arsenic applications in many fields. In particular, theoretical calculations have also predicted some exotic properties of 2D arsenic materials, endowing great impetus for the development and discovery of more possible applications of 2D arsenene and arsenic. To date, 2D arsenene and arsenic have been found to have rich applications, such as FET, biology, sensor, and luminescence applications. In this section, we will specifically introduce the applications of 2D arsenene and arsenic reported recently.

4.1. FETs

Natural minerals with an orthorhombic crystal structure (puckered arsenic) and weak interlayer forces provide great convenience for the exfoliation of black arsenic.[119] Chen et al. achieved thin black arsenic nanosheets via mechanical exfoliation, fabricated black arsenic devices and systematically investigated the thermal and electric transport anisotropies along the AC and ZZ directions.[46] The FET based on few-layer black arsenic with a thickness of 3.1 nm exhibited p-type behavior, with a mobility of 90 $cm^2\ V^{-1}\ s^{-1}$ and an on/off ratio of 10^4 (**Figure 12**a–c).[46] Zhong et al. investigated the transport properties and stability of monolayer and few-layer black arsenic nanosheets.[38] They found that the performances of black arsenic-based FETs strongly depend on the thickness (Figure 12d,e).[38] The FETs exhibited the highest carrier mobility of ≈59 $cm^2\ V^{-1}\ s^{-1}$ for a thickness of ≈5.7 nm and the largest on/off ratio exceeding 10^5 for 4.6 nm thick black arsenic.[38] Temperature-dependent measurements of carrier mobilities showed that the carrier mobility was mainly confined by the scattering of impurities at low temperatures but limited by lattice scattering at high temperatures.[38] Most recently, our group realized the transition of semimetallic gray arsenene into semiconductive vitreous

arsenene via a wet chemistry method.[80] The FETs based on completely vitrified arsenene were also fabricated, as shown in Figure 12f,g. Different from semimetal gray arsenene, the FETs based on vitreous arsenene nanoflakes show a carrier mobility of ≈159.1 $cm^2\ V^{-1}\ s^{-1}$, demonstrating a typical p-type semiconducting behavior.[80]

The thick (multilayer) 2D gray arsenic shows semimetal features and excellent conductivity. Theoretical calculations demonstrated that monolayer or bilayer gray arsenene demonstrates the emergence of bandgaps. However, due to the air sensitivity and preparation difficulty of mono- or bilayer gray arsenene, FETs of gray arsenene have not yet been experimentally fabricated, and their performances and characteristics have only been investigated by several works via theoretical calculations.[54,56,120] Pizzi et al. carried out a multiscale simulation of monolayer arsenene and antimonene FETs to investigate their transport and output properties (**Figure 13**a,b).[56] They studied the influence of the short-channel effects and underlap doping concentrations of the source and drain on the performances of arsenene- and antimonene-based metal oxide semiconductor FETs (MOSFETs).[56] Then, they compared the performances of double gate MOSFETs using monolayer arsenene and antimonene as channels to satisfy industry requirements, finding that those MOSFETs potentially achieve the target set by the International Technology Roadmap for Semiconductors (ITRS) for high-performance digital applications.[56] Subsequently, by using accurate ab initio methods, Wang et al. investigated the many-body effect, carrier mobility, and device performance of single-layer buckled (gray) arsenene and antimonene.[54] For the three different electron doping concentrations between 10^{13} and 10^{14} cm^{-2} of a double gate MOSFET based on monolayer arsenene with a gate length of 10 nm, the transfer characteristics show a subthreshold swing (SS) of 53–55 mV dec^{-1} (Figure 13c), satisfying both the low-power (LP) and high-power (HP) applications in all the studied nodes.[54] By using ab initio electronic calculations and quantum transport simulations, Wang et al. also studied the electrical contact interactions of monolayer gray arsenene with different electrodes.[120] They found that the Schottky barrier between gray arsenene and bulk metal contacts can be suppressed by introducing 2D graphene. In particular, a monolayer arsenene device demonstrated barrier-free hole injection while using a graphene-Pt hybrid electrode.[120] The remarkable performance of gray arsenene investigated by theoretical simulations manifests its great potential for applications in FETs.

Experimentally reported carrier mobilities of black arsenene are at the level of tens of $cm^2\ V^{-1}\ s^{-1}$ with considerable on/off ratios (≈10^5). The FETs of monolayer gray arsenene have not been reported yet, and the devices of gray arsenene with several nanometers thick show semimetallic characteristics. Notably, there is still plenty of room for improving the performance of arsenene-based FETs. For example, the construction of interlaced black arsenene and gray arsenene nanostructure may be a potential strategy to obtain high-performance devices, which could simultaneously combine the switching effect of black arsenene and the high conductivity of gray arsenene. Besides, the theoretically calculated high carrier mobility of monolayer gray arsenene and the remarkable performance of simulated gray arsenene MOSFETs call for further experimental explorations. All of these discussions suggest that arsenene has great potential in achieving high-speed FETs.

4.2. Photoluminescence

Tsai et al. estimated the bandgap of multilayer gray arsenene nanoribbons by measuring the PL spectrum.[58] They inhibited the trapping of defect states by lowering the temperature, and then, a series of measurements were carried out at different temperatures. As illustrated in **Figure 14**a, a weak PL peak centered at ≈540 nm was observed in the PL spectrum at 150 K. When the temperature dropped from 150 to 105 K, the PL intensity increased by three times. The PL intensity increased to ≈6×10^5 when the temperature was reduced to 90 K, and the bright green light emission is shown in the inset of Figure 14a. The green light emission with a wavelength of 540 nm corresponded to a bandgap of ≈2.3 eV for multilayer arsenene. The prepared arsenene nanoribbons are multilayer rather than bilayer or monolayer. According to previous computational works, the bandgap opening of arsenene only occurred when the layer number was below 2. The authors explained that the emergence of the band gap of multilayer arsenene nanoribbons may be attributed to the quantum confinement effect and the turbostratic stacking of the arsenene layer (such as AA stacking).[58] However, no PL peaks were detected from the thicker (≈21.4 nm) arsenene nanoribbons, suggesting that the metallic to semiconductor transformation occurred at thicknesses of ≈14 to ≈21.4 nm.

4.3. Thermal Conductivity and Photothermal Effects

2D black arsenic exhibited anisotropic thermal transport properties.[46] Chen et al. constructed a representative device of a black arsenic nanoribbon with two suspended pads (Figure 14b).[46] By transporting heat from the heater to the sensor, the thermal conductivity κ can be measured and is illustrated in Figure 14c. The measured κ values of the ZZ direction and AC direction are different. κ along the ZZ direction is higher than that along the AC direction, giving a κ ratio of ≈1.6 and demonstrating the anisotropic thermal transport property of black arsenic.

The photothermal effect of 2D black and gray arsenic has also been investigated using 880 nm laser irradiation.[62] The temperatures of arsenic nanosheet dispersions with three different concentrations and pure water were then tested. All arsenic dispersions exhibited fast temperature increases in the first 5 min, while pure water showed negligible temperature fluctuations. The relatively larger concentrations correspondingly gave higher temperatures after laser irradiation. Finally, the temperature increased gradually and finally reached a maximum temperature. After 20 min of laser irradiation and at concentrations of 0.1, 0.25, and 1 mg mL^{-1}, the temperature of the gray arsenic dispersions increased from room temperature to 52, 55, and 58 °C, and black arsenic reached temperatures of 45, 51, and 56 °C, respectively (Figure 14d).[62]

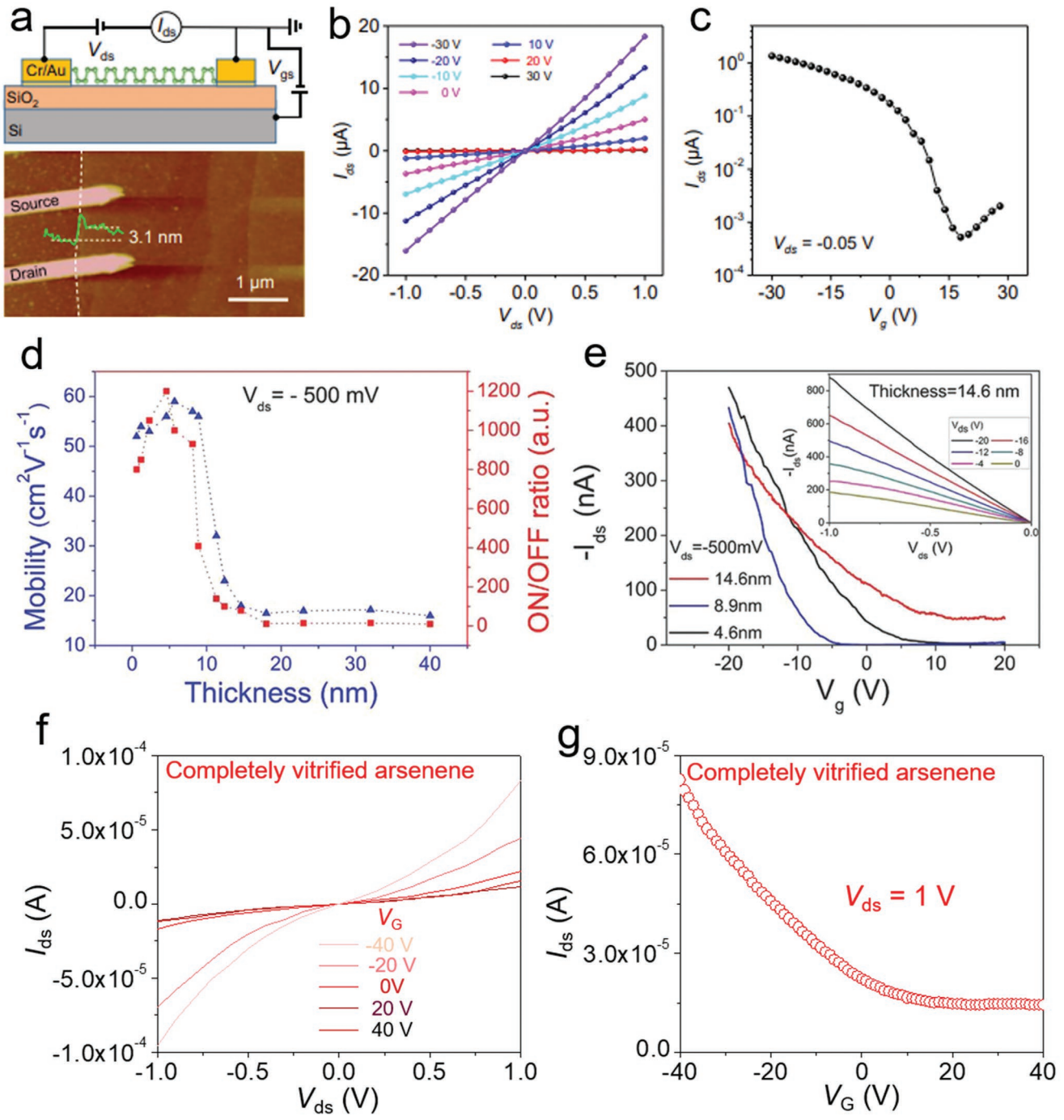

Figure 12. a) Schematic (upper) and AFM image (below) of a 3.1 nm thick black arsenic-based FET. b,c) Corresponding output and transfer curves of the FET in (a). a–c) Reproduced with permission.[46] Copyright 2018, John Wiley & Sons, Inc. All rights reserved. d) Thickness-dependent carrier mobilities and on/off ratios of black arsenic FETs. e) Transfer curves of three black arsenic FETs with thicknesses of 4.6, 8.9, and 14.6 nm. d,e) Reproduced with permission.[38] Copyright 2018, WILEY-VCH Verlag GmbH & Co. KGaA, Weinheim. f,g) Output characteristic curves and transfer characteristic curve of completely vitrified arsenene-based FETs. f,g) Reproduced with permission.[80] Copyright 2021, WILEY-VCH Verlag GmbH & Co. KGaA, Weinheim.

4.4. Chemical Sensing and Electrocatalysis

Moreover, impedimetric sensors based on the prepared 2D black and gray arsenene materials were also fabricated to detect volatile organic compounds (VOCs), demonstrating that 2D gray arsenic can be sensitive to methanol and ethanol and that 2D black arsenic can respond to five VOCs.[62] Beladi-Mousavi et al. constructed vapor sensors based on 2D arsenene nanosheets prepared by liquid-phase exfoliation.[43] By using electrochemical impedance spectroscopy as a study tool, changes in electronic properties were explored (**Figure 15**a).[43] The fabricated gas detectors were selectively sensitive to methanol or acetone

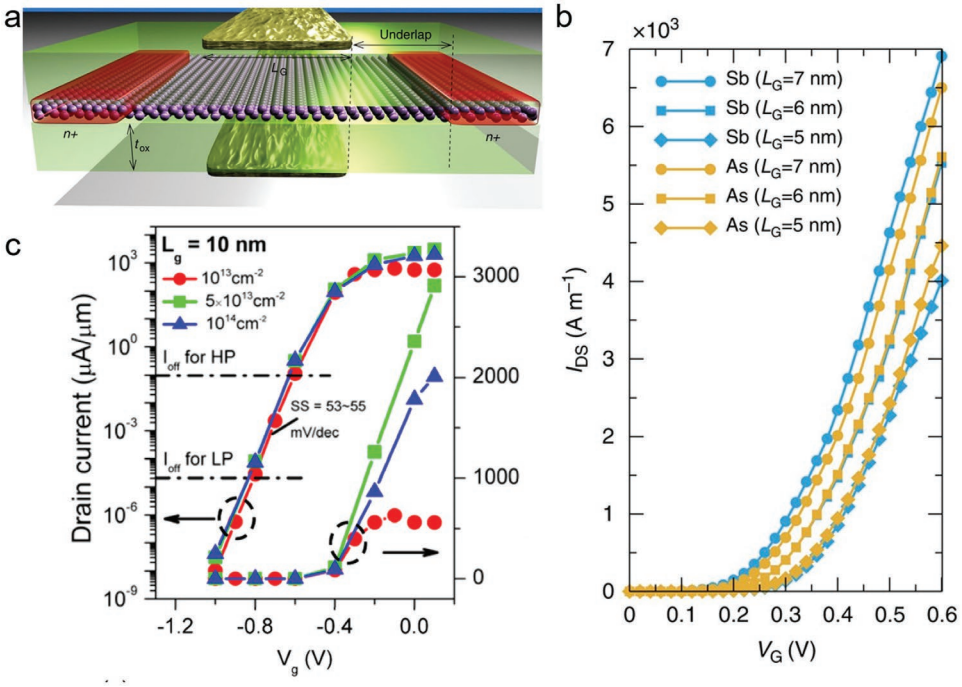

Figure 13. a) Schematic illustration of a double gate n-doped MOSFET prepared using monolayer gray arsenene as a channel. b) Transfer curves of arsenene- and antimonene-based MOSFETs with different gate lengths. a,b) Reproduced with permission.[56] Copyright 2020, Springer Nature Limited. c) Transfer characteristics of a double gate MOSFET based on monolayer arsenene with different source and drain electron doping concentrations. The gate length is 10 nm. c) Reproduced with permission.[54] Copyright 2017, American Chemical Society.

vapors with a fast response (Figure 15b,c). Moreover, sensors illustrated good durability with only small phase shifts during the detection of methanol vapors. These results indicate the great potential of 2D arsenene and arsenic materials in the application of gas sensors. Based on previous reports, the presence of oxidizing or reducing gases can effectively influence the resistance of MoO_3 nanobelt-based sensors, which can be attributed to the absorption of oxygen molecules induced free electrons capture from conduction band.[121] The 2D arsenene and arsenic materials are also sensitive to oxygen, indicating the possibility of arsenene in sensing oxidizing or reducing gases. Compared with other nanomaterials, such as MoO_3 nanobelts, nanocomposite networks of polyaniline and carbon nanotubes, MXene and so on, the arsenene-based gas sensors are usually unstable and not environmentally friendly,[121–123] which might not bear relative strong reductive and oxidizing gases and harsh environmental conditions, and might suffer from chemical degradation and valence state changes.[123] However, the high sensitivity of arsenene toward oxidation and reductive agents hints that arsenene may be an important candidate in fabricating high-sensitivity gas sensors. Combining arsenene with other stable and conductive materials to construct sensors could be a promising choice. Moreover, arsenene also shows distinct biological properties compared with other pnictogens, suggesting a lot of possibilities for developing biomolecular detectors. Overall, although the sensors based on 2D arsenene and arsenic materials are rarely investigated, it can be anticipated that the gas or biomolecular sensors based on 2D arsenene and arsenic materials may have great potential for some special purposes.

In addition, 2D arsenic has been applied to electro-catalytical reactions such as the hydrogen evolution reaction (HER), oxygen reduction reaction (ORR), and oxygen evolution reaction (OER).[44] Pumera et al. investigated the HER polarization curves of pnictogens obtained with bulk and nanosheet forms in acidic and alkaline solutions.[44] The onset voltage of gray arsenic nanosheets (–0.98 V vs reversible hydrogen electrode (RHE)) is larger than that of bulk arsenic (≈–1.7 V vs RHE) in acidic media (Figure 15d). Moreover, in both acidic and alkaline media, the HER performance of pnictogen nanosheets is typically improved compared to that of its bulk crystals, indicating that the exfoliation of arsenic can effectively increase the number of active sites and enhance the catalytic properties. In addition, they also studied the OER electrocatalytic activity of arsenic nanosheets and bulk arsenic.[44] The polarization curves of arsenic nanosheets in alkaline media showed less improvement in performance with respect to the HER but maintained a similar trend. However, the ORR tests of arsenic nanosheets in 1.0 M KOH displayed nearly unchanged potentials with respect to those of the bare glassy carbon (GC) electrode, indicating that the arsenic nanosheets have weak catalytic activity for the ORR.[44]

4.5. Biomedical Applications

Monoelemental 2D materials, such as graphene, black phosphorus, antimonene, and borophene, have been demonstrated to be particularly promising materials with extraordinary physicochemical properties and biocompatibility for biological

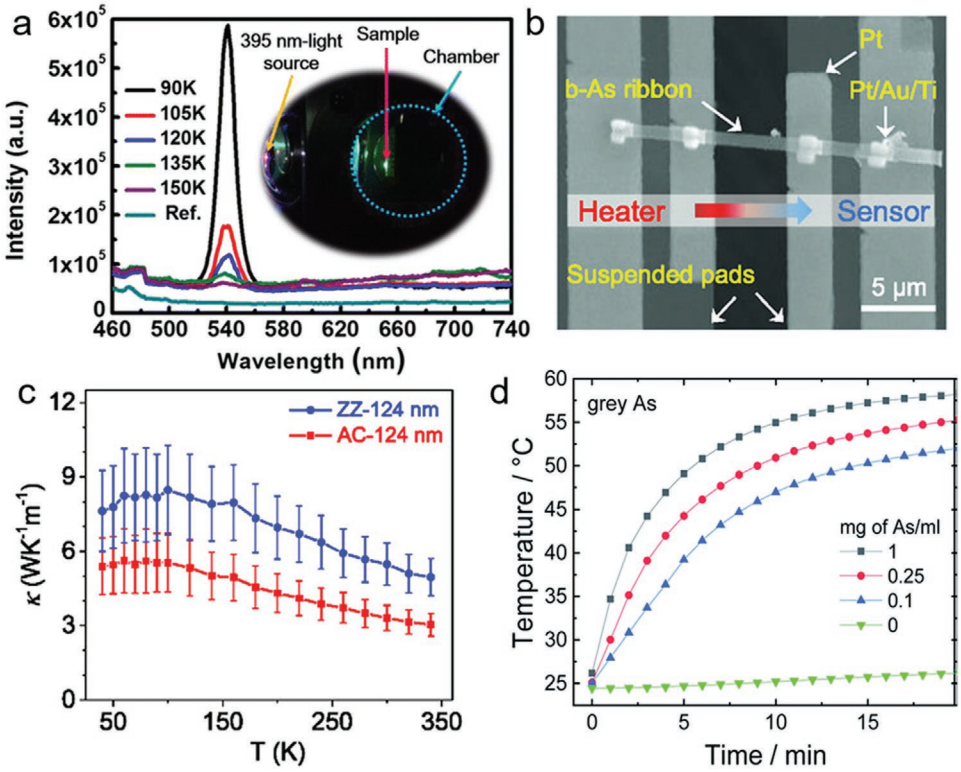

Figure 14. a) The observed PL spectra of multilayer gray arsenene nanoribbons on the InN/InAs substrate at different temperatures. Reproduced with permission.[58] Copyright 2020, American Chemical Society. b) Thermal conductivity measurements of a suspended black arsenic device. c) Thermal conductivity as a function of the temperature of black arsenic nanoribbons along the ZZ and AC directions. b,c) Reproduced with permission.[46] Copyright 2018, WILEY-VCH Verlag GmbH & Co. KGaA, Weinheim. d) Photothermic effect of black and gray arsenic suspensions with different concentrations. Reproduced with permission.[62] Copyright 2020, The Royal Society of Chemistry.

applications.[119,124–128] 2D arsenene and arsenic have also shown interesting potential for biological applications as enzymatic phenol biosensors, cytotoxicity agents, and therapeutic agents for acute promyelocytic leukemia (APL) cells.[23,39,117] Moreover, the toxicity of arsenene and 2D arsenic materials is also discussed. Yellow arsenic is commonly with high toxicity, while gray and black arsenic in elementary substance forms are less toxic. It can be assumed that toxicity of 2D gray and black arsenene are relatively weak.[117] Besides, 2D arsenene and arsenic materials prepared by liquid-phase exfoliation method show excellent therapeutic effect toward APL cancer cells.[39] The presented toxicity of arsenene may be attributed to the oxidization of arsenene in NB4 cancer cells, which can be identified by Raman spectrum of arsenene-treated NB4 cells.[39] More recently, Liu et al. demonstrated that DSPE-mPEG-modified arsenene shows high toxicity toward cancer cells, but much less toxicity in normal cells.[66] The distinct toxicities of arsenene in cancer cells and normal cells are ascribed to the valence increase of arsenic activated by cancer cell, reducing superoxide dismutase (SOD) activity and producing massive reactive oxygen species (ROS).

Mayorga-Martinez et al. found that shear-force exfoliated 2D pnictogens (phosphorene, arsenene, antimonene, and bismuthine) can well detect phenols with high sensitivity and selectivity (**Figure 16**a).[23] The biosensor was prepared on a GC electrode by coating pnictogen nanosheets, tyrosinase (Tyr), and glutaraldehyde (Glu). Chia et al. studied the cytotoxicity of pnictogen nanosheets (As, Sb, and Bi) toward adenocarcinoma human lung epithelial A549 cells (Figure 16b).[117] The arsenic nanosheets demonstrated the highest toxicity among the pnictogen nanosheets, suggesting that 2D arsenic nanosheets have the potential to inhibit the viability and reproduction of A549 cells and that low-toxicity 2D antimonene and bismuthine nanosheets have potential for use in drug delivery.[117]

Moreover, our recent work found that arsenene nanosheets could be applied in anticancer studies.[39] 2D arsenene nanosheets were prepared by sonicating bulk arsenic crystals in DMSO solvents. Then, the cytotoxicity of arsenene nanosheets to five cancer cell lines (A2780, A549, HeLa, MCF-7 cancer cells, and the human normal liver cell line (L-02)) was investigated (Figure 16c). We found that arsenene nanosheets at a concentration of 1.2 μg mL^{-1} are an effective therapeutic agent toward NB4 promyelocytic leukemia (APL) cells, with 80% inhibition (Figure 16c).[39] In contrast, the arsenene nanosheets showed no toxicity to normal L-02 cells, suggesting the high selectivity of arsenene nanosheets. A detailed mechanistic investigation of NB4 cells confirmed that the depolarization of mitochondrial membrane potentials and the generation of ROS are the reasons for the apoptosis of NB4 cells. Detailed proteomic profiling analysis suggested that arsenene nanosheets mainly act on nuclear DNA and target the nuclear protein TXNL1 in NB4 cells, suppressing replication, nucleotide excision repair,

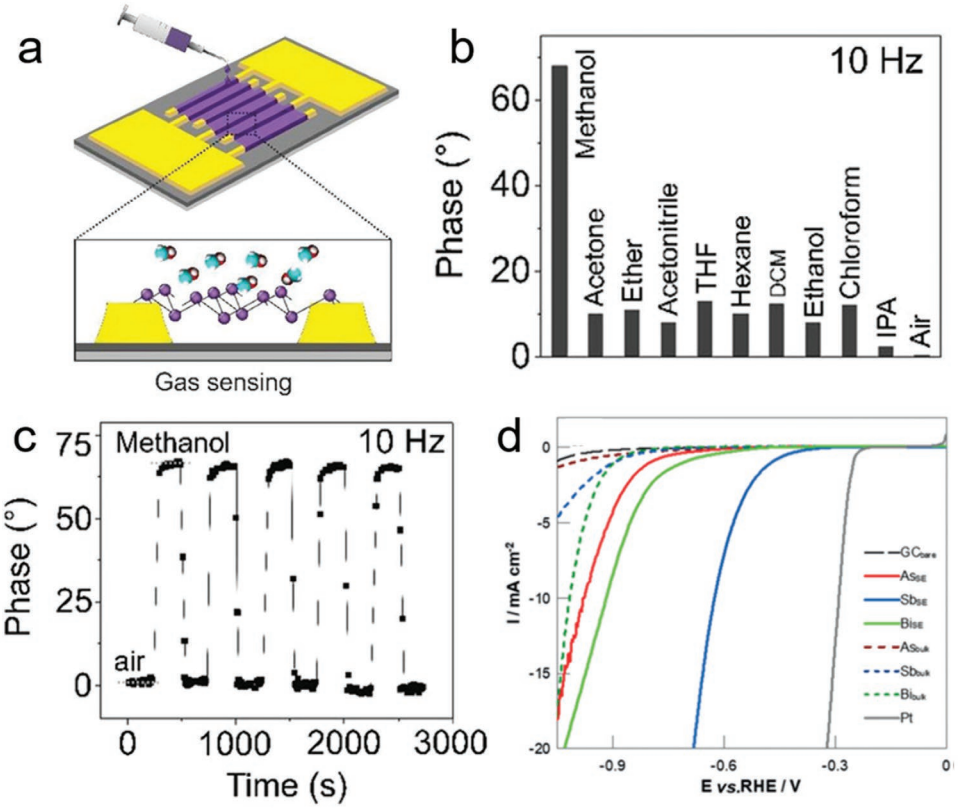

Figure 15. a) Schematic of 2D arsenic nanosheet-based vapor sensors. b) The value of the impedance phase of the vapor sensors in the presence of various solvents at 10 Hz. c) Time-dependent phase evolution of a 2D arsenic-based sensor for methanol detection. a–c) Reproduced with permission.[43] Copyright 2019, WILEY-VCH Verlag GmbH & Co. KGaA, Weinheim. d) Linear sweep voltammetry (LSV) curves of pnictogen in 0.5 M H_2SO_4. Reproduced with permission.[44] Copyright 2017, Wiley-VCH Verlag GmbH & Co. KGaA, Weinheim.

and pyrimidine metabolism pathways (Figure 16d,f).[39] The arsenene nanosheets tend to bind with nuclear nucleotide acid binding proteins and further destroy the nuclei. Moreover, we tested in vivo toxicity in mice and found that arsenene nanosheets are biosafe (Figure 16e).

More recently, Liu et al. have prepared DSPE-mPEG-modified arsenene nanodots via liquid-phase exfoliation method using Vitamin C to protect arsenene from oxidization.[66] The resulted arsenene nanodots@PEG composites depict obviously different toxicities toward cancer cells and normal cells. They identified that the selective killing effect was attributed to the transformation of arsenene from less toxic As^0 to severe toxic oxidation states, resulting in decreased SOD activity and increased ROS that further lead to mitochondrial damage, cell-cycle arrest, and DNA damage (**Figure 17**).[129] Moreover, in vivo experiments further demonstrated the suppressed growth of solid tumors by arsenene nanodots@PEG and long-term biocompatibility in healthy tissues even at high doses and repetitive administration.[129]

The manifested contrast toxicities of arsenene in cancer cells and normal cells suggest its great prospect in biological applications. It is well known that arsenic oxide-based agentia can serve as clinical medicines for the therapy of APL cancer cells, while the contradiction between the therapeutic efficacy and the systemic toxicity is a distinct concern. The fantastic biological properties of arsenene may eliminate this contradiction, providing a great promise of arsenene in clinic applications. On the one hand, the arsenene has relatively weak toxicity to normal organisms, ensuring the safety of human body during medical applications. On the other hand, the arsenene presents great toxicity in cancer cells and can effectively kills cancer cells, suggesting a good targeting effect. There, it is vital in preventing the oxidation of 2D arsenene and arsenic materials during preparation and preservation processes. Effective anti-oxidation strategies could be very helpful for the development of arsenene toward practical biological applications.

5. Challenges and Perspectives

In this review, the recent advances of 2D arsenene and arsenic, including fundamental properties, preparation, and applications, are summarized. With the developments made in the past few years, 2D arsenene and arsenic have been successfully prepared, and their optical and electrical properties have been intensively investigated. Mechanical exfoliation, epitaxial growth, and liquid-phase exfoliation were performed for the experimental realization of 2D arsenene and arsenic. Atom-thick, high-yield, and high crystal quality 2D arsenene and arsenic were prepared. 2D arsenene and arsenic with different phases or thicknesses exhibit distinguishing electrical and optical properties. The chemical and environmental stabilities

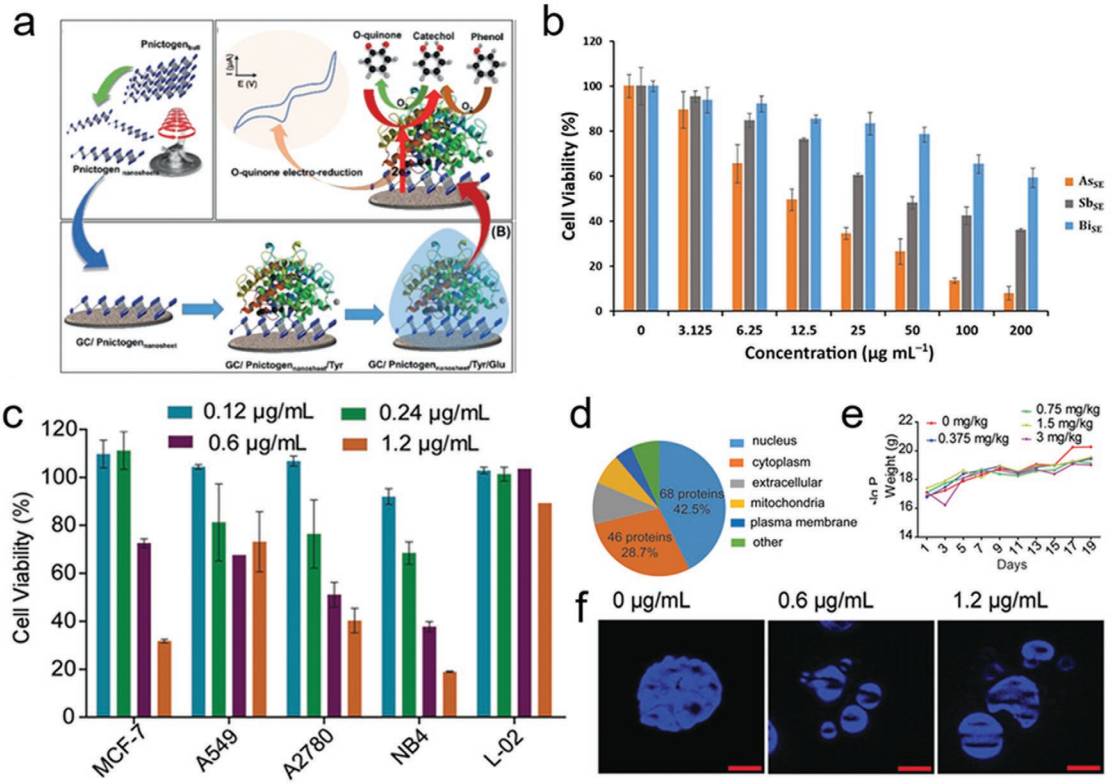

Figure 16. a) Schematic illustration of enzymatic phenol biosensors based on 2D pnictogen nanosheets. a) Reproduced with permission.[23] Copyright 2019, Wiley-VCH Verlag GmbH & Co. KGaA, Weinheim. b) The viability of A549 cells as a function of concentrations of pnictogen nanosheets investigated via MTT assays. b) Reproduced with permission.[117] Copyright 2019, John Wiley & Sons, Inc. All rights reserved. c) The resulting viability of different cells treated with various concentrations of arsenene nanosheets. d) Differentially expressed proteins of arsenene-treated cells. e) The recorded body weights of mice after the injection of arsenene nanosheets. f) Nuclear images of NB4 cells before and after treatment with arsenene nanosheets. c–f) Reproduced with permission.[39] Copyright 2020, John Wiley & Sons, Inc. All rights reserved.

of 2D arsenene and arsenic are also investigated in detail, and protection strategies are correspondingly developed. In particular, those methods used for the production of 2D arsenene and arsenic, with their respective merits and defects, are complementary to the various applications relating to transistors, biological applications, electrocatalysis, sensors, and so on. Moreover, the 2D arsenene and arsenic materials also presented outstanding advantages compared with other 2D materials, such as naturally existed metal and semiconductor phases, controllable metal-to-semiconductor transition, and contrast toxicities in cancer cells and normal cells.

However, exploration is just the beginning for young arsenene. The synthesis process is uncontrolled, studies on properties are insufficient, and the development of applications is in its infancy, indicating that arsenene is far from being ready for practical applications. The main challenges lie in mass production, thickness, and phase control, property manipulation, and application development. Next, we will detailly discuss the current challenges of 2D arsenene and arsenic and provide some related perspectives.

1) The preparation of 2D arsenene and arsenic materials with uniform thickness and controllable layer number is still a notable challenge. Theoretical calculations have predicted that the exotic properties of arsenene are primarily based on monolayer arsenene. Although 2D arsenene and arsenic nanocrystals have been successfully synthesized, the as-prepared samples generally have a relatively large range of thickness and rarely contain monolayer or bilayer. Especially, for gray arsenic, the metallic character and relatively stronger interlayer interaction make it difficult to obtain thin arsenene crystals with controllable thickness via mechanical exfoliation or liquid-phase exfoliation. To date, functional devices based on monolayer gray arsenene, such as FETs and photodetectors, are still lacking. Apparently, the preparation of arsenene with different thickness will bring distinctive properties, which is helpful for realizing various types of functional devices. Thus, the controllable realization of monolayer and thickness-controllable arsenene are of great significance for verifying related theoretical predictions and supporting the development of deice applications.
2) The environmental instability of 2D arsenene and arsenic still needs to be overcome. In particular, gray arsenene exhibits worse ambient stability than black arsenene. In addition, the instability of arsenene considerably increases while the thickness decreases, greatly hindering further property studies, device processing, and sample storage. Therefore, developing a repeatable and effective method to passivate arsenene without destroying its intrinsic properties is another core problem in the development of arsenene.

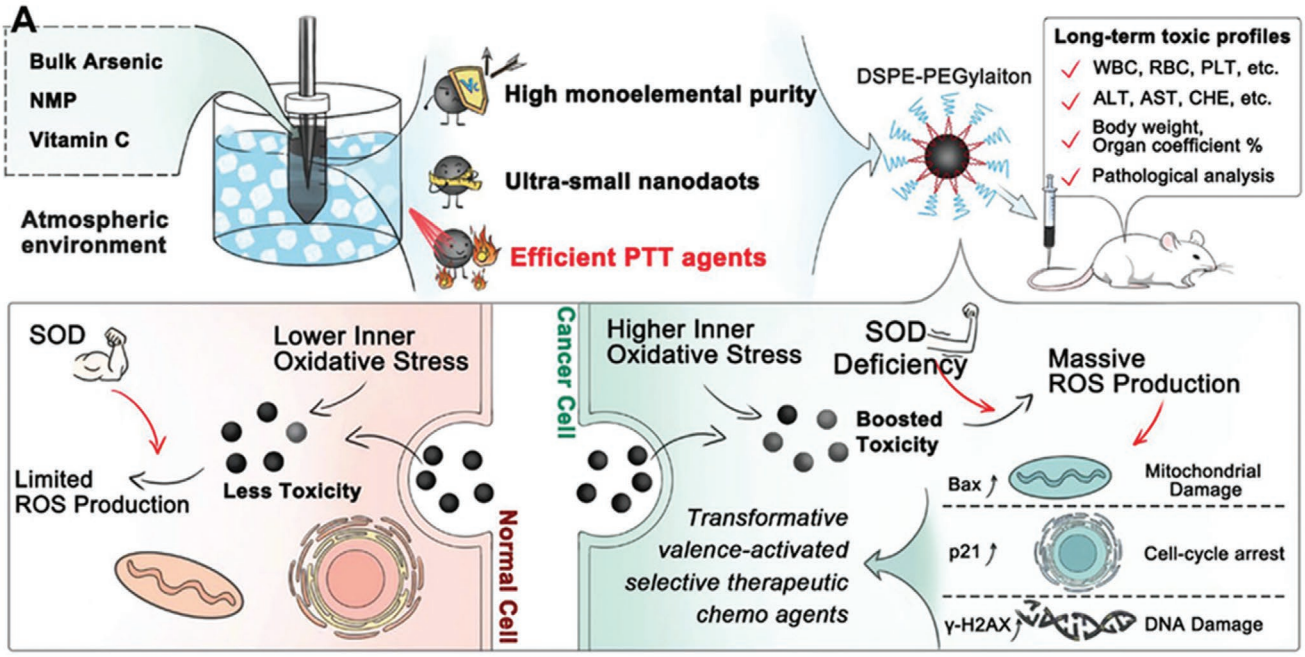

Figure 17. Schematic illustration of DSPE-mPEG modified arsenene applied to normal cells and cancer cells. Reproduced with permission.[66] Copyright 2021, Wiley-VCH Verlag GmbH & Co. KGaA, Weinheim.

3) Environmentally friendly and low-cost strategies for the mass production of 2D arsenene and arsenic with gram-level or chip-level yields are also a challenge that deserves mention. The most commonly used precursors currently are arsenic crystals (commercial or natural), which are of little harm and toxicity to the human body. However, the preparation processes, such as processes exploiting sonication waves and high temperatures, usually involve high energy and organic solvents, which usually result in toxic gases or liquid-phase products. Although liquid-phase exfoliation can generate gram-level 2D arsenene and arsenic powders, the thickness and size are uncontrollable, requiring further optimization of the experimental conditions and installation. Moreover, the preparation of large-area 2D arsenene and arsenic at the chip level is still stagnant, while wafer-size 2D materials are the foundation for future commercialization and industrialization. Hence, developing environmentally friendly and low-cost experimental methods to prepare large-scale and high-yield 2D arsenene and arsenic contributes to the advancement of 2D arsenene and arsenic.
4) Studies of fundamental properties and the development of critical applications are still insufficient for 2D arsenic materials, especially for atom-thick arsenene. As a limitation of arsenene preparation, research on the intrinsic properties and applications of 2D arsenene and arsenic is just the tip of the iceberg. For a few simple examples, studies on using few-layer or monolayer arsenene to obtain energy storage devices, photodetectors, photovoltaic devices, catalysts, spin quantum effects, thermoelectricity and so on have not yet been realized or reported. These gaps in the applications and properties of novel arsenene suggest great opportunities and possibilities and formidable difficulties and challenges.

Thus, more focus on the preparation of arsenene is necessary, especially for gray arsenene, which is hardly achieved by mechanical exfoliation. Chemical (physical) vapor deposition and molecular beam epitaxy may be good choices for obtaining single-crystal arsenene for intrinsic property studies and device fabrication. Accordingly, the regulation of experimental parameters, selection of suitable substrates, and improvement of instrument stability are of great importance for the growth of arsenene with repeatable location, uniformity, and thickness. In addition, some mature thin-film preparation technologies (atomic layer deposition, thermal evaporation, magnetron sputtering, metal organic chemical vapor deposition, and so on) may be good alternative methods for chip-level preparation of 2D arsenene. Moreover, surface functionalization and inert material coatings or doping are considerable ways to protect and simultaneously regulate the properties of arsenene.

Acknowledgements

This work was supported by the National Key Research and Development Program of China (2017YFA0208200), the Fundamental Research Funds for the Central Universities of China (0205-14380266), the National Natural Science Foundation of China (22022505 and 21872069), the Natural Science Foundation of Jiangsu Province (BK20180008), and the Shenzhen Fundamental Research Program of Science, Technology and Innovation Commission of Shenzhen Municipality (JCYJ20180307155007589).

Conflict of Interest

The authors declare no conflict of interest.

Keywords

2D arsenic, 2D materials, arsenene, controlled preparation, functional devices, fundamental properties

Received: July 31, 2021
Revised: October 6, 2021
Published online:

[1] Q. H. Wang, K. Kalantar-Zadeh, A. Kis, J. N. Coleman, M. S. Strano, *Nat. Nanotechnol.* **2012**, *7*, 699.
[2] M. Chhowalla, H. S. Shin, G. Eda, L. J. Li, K. P. Loh, H. Zhang, *Nat. Chem.* **2013**, *5*, 263.
[3] K. S. Novoselov, D. Jiang, F. Schedin, T. J. Booth, V. V. Khotkevich, S. V. Morozov, A. K. Geim, *Proc. Natl. Acad. Sci. U. S. A.* **2005**, *102*, 10451.
[4] K. S. Novoselov, A. K. Geim, S. V. Morozov, D. Jiang, Y. Zhang, S. V. Dubonos, I. V. Grigorieva, A. A. Firsov, *Science* **2004**, *306*, 666.
[5] A. Molle, J. Goldberger, M. Houssa, Y. Xu, S. C. Zhang, D. Akinwande, *Nat. Mater.* **2017**, *16*, 163.
[6] A. J. Mannix, B. Kiraly, M. C. Hersam, N. P. Guisinger, *Nat. Rev. Chem.* **2017**, *1*, 0014.
[7] B. Guo, Q. l. Xiao, S. h. Wang, H. Zhang, *Laser Photonics Rev.* **2019**, *13*, 1800327.
[8] D. Tyagi, H. Wang, W. Huang, L. Hu, Y. Tang, Z. Guo, Z. Ouyang, H. Zhang, *Nanoscale* **2020**, *12*, 3535.
[9] Z. Y. Cai, B. L. Liu, X. L. Zou, H. M. Cheng, *Chem. Rev.* **2018**, *118*, 6091.
[10] J. P. Lu, H. W. Liu, E. S. Tok, C. H. Sow, *Chem. Soc. Rev.* **2016**, *45*, 2494.
[11] C. Anichini, W. Czepa, D. Pakulski, A. Aliprandi, A. Ciesielski, P. Samori, *Chem. Soc. Rev.* **2018**, *47*, 4860.
[12] C. Dun, C. A. Hewitt, Q. Li, J. W. Xu, D. C. Schall, H. Lee, Q. Jiang, D. L. Carroll, *Adv. Mater.* **2017**, *29*, 1700070.
[13] A. Gupta, T. Sakthivel, S. Seal, *Prog. Mater. Sci.* **2015**, *73*, 44.
[14] H. Liu, A. T. Neal, Z. Zhu, Z. Luo, X. F. Xu, D. Tomanek, P. D. Ye, *ACS Nano* **2014**, *8*, 4033.
[15] A. H. Castro Neto, F. Guinea, N. M. R. Peres, K. S. Novoselov, A. K. Geim, *Rev. Mod. Phys.* **2009**, *81*, 109.
[16] X. F. Qian, J. W. Liu, L. Fu, J. Li, *Science* **2014**, *346*, 1344.
[17] G. Fiori, F. Bonaccorso, G. Iannaccone, T. Palacios, D. Neumaier, A. Seabaugh, S. K. Banerjee, L. Colombo, *Nat. Nanotechnol.* **2014**, *9*, 768.
[18] C. L. Tan, X. H. Cao, X. J. Wu, Q. Y. He, J. Yang, X. Zhang, J. Z. Chen, W. Zhao, S. K. Han, G. H. Nam, M. Sindoro, H. Zhang, *Chem. Rev.* **2017**, *117*, 6225.
[19] S. Z. Butler, S. M. Hollen, L. Y. Cao, Y. Cui, J. A. Gupta, H. R. Gutierrez, T. F. Heinz, S. S. Hong, J. X. Huang, A. F. Ismach, E. Johnston-Halperin, M. Kuno, V. V. Plashnitsa, R. D. Robinson, R. S. Ruoff, S. Salahuddin, J. Shan, L. Shi, M. G. Spencer, M. Terrones, W. Windl, J. E. Goldberger, *ACS Nano* **2013**, *7*, 2898.
[20] L. Britnell, R. M. Ribeiro, A. Eckmann, R. Jalil, B. D. Belle, A. Mishchenko, Y. J. Kim, R. V. Gorbachev, T. Georgiou, S. V. Morozov, A. N. Grigorenko, A. K. Geim, C. Casiraghi, A. H. Castro Neto, K. S. Novoselov, *Science* **2013**, *340*, 1311.
[21] Y. J. Gong, J. H. Lin, X. L. Wang, G. Shi, S. D. Lei, Z. Lin, X. L. Zou, G. L. Ye, R. Vajtai, B. I. Yakobson, H. Terrones, M. Terrones, B. K. Tay, J. Lou, S. T. Pantelides, Z. Liu, W. Zhou, P. M. Ajayan, *Nat. Mater.* **2014**, *13*, 1135.
[22] K. S. Novoselov, A. Mishchenko, A. Carvalho, A. H. C. Neto, *Science* **2016**, *353*, aac9439.
[23] C. C. Mayorga-Martinez, R. Gusmao, Z. Sofer, M. Pumera, *Angew. Chem., Int. Ed.* **2019**, *58*, 134.
[24] M. Z. Mohamad Nasir, M. Pumera, *TrAC, Trends Anal. Chem.* **2019**, *121*, 115696.
[25] S. Guo, Y. Zhang, Y. Ge, S. Zhang, H. Zeng, H. Zhang, *Adv. Mater.* **2019**, *31*, 1902352.
[26] S. Zhang, S. Guo, Z. Chen, Y. Wang, H. Gao, J. Gomez-Herrero, P. Ares, F. Zamora, Z. Zhu, H. Zeng, *Chem. Soc. Rev.* **2018**, *47*, 982.
[27] M. Pumera, Z. Sofer, *Adv. Mater.* **2017**, *29*, 1605299.
[28] W. H. Zhou, J. Y. Chen, P. X. Bai, S. Y. Guo, S. L. Zhang, X. F. Song, L. Tao, H. B. Zeng, *Research* **2019**, *2019*, 1046329.
[29] P. Ares, J. J. Palacios, G. Abellan, J. Gomez-Herrero, F. Zamora, *Adv. Mater.* **2018**, *30*, 1703771.
[30] Y. Hu, Z.-H. Qi, J. Lu, R. Chen, M. Zou, T. Chen, W. Zhang, Y. Wang, X. Xue, J. Ma, Z. Jin, *Chem. Mater.* **2019**, *31*, 4524.
[31] Y. Xu, Z. Shi, X. Shi, K. Zhang, H. Zhang, *Nanoscale* **2019**, *11*, 14491.
[32] W. Tao, N. Kong, X. Y. Ji, Y. P. Zhang, A. Sharma, J. Ouyang, B. W. Qi, J. Q. Wang, N. Xie, C. Kang, H. Zhang, O. C. Farokhzad, J. S. Kim, *Chem. Soc. Rev.* **2019**, *48*, 2891.
[33] F. Li, M. Xue, J. Li, X. Ma, L. Chen, X. Zhang, D. R. MacFarlane, J. Zhang, *Angew. Chem., Int. Ed.* **2017**, *56*, 14718.
[34] L. K. Li, Y. J. Yu, G. J. Ye, Q. Q. Ge, X. D. Ou, H. Wu, D. L. Feng, X. H. Chen, Y. B. Zhang, *Nat. Nanotechnol.* **2014**, *9*, 372.
[35] L. Lu, X. Tang, R. Cao, L. Wu, Z. Li, G. Jing, B. Dong, S. Lu, Y. Li, Y. Xiang, J. Li, D. Fan, H. Zhang, *Adv. Opt. Mater.* **2017**, *5*, 1700301.
[36] F. Reis, G. Li, L. Dudy, M. Bauernfeind, S. Glass, W. Hanke, R. Thomale, J. Schafer, R. Claessen, *Science* **2017**, *357*, 287.
[37] H. T. Yuan, X. G. Liu, F. Afshinmanesh, W. Li, G. Xu, J. Sun, B. Lian, A. G. Curto, G. J. Ye, Y. Hikita, Z. X. Shen, S. C. Zhang, X. H. Chen, M. Brongersma, H. Y. Hwang, Y. Cui, *Nat. Nanotechnol.* **2015**, *10*, 707.
[38] M. Zhong, Q. Xia, L. Pan, Y. Liu, Y. Chen, H.-X. Deng, J. Li, Z. Wei, *Adv. Funct. Mater.* **2018**, *28*, 1802581.
[39] X. Wang, Y. Hu, J. Mo, J. Zhang, Z. Wang, W. Wei, H. Li, Y. Xu, J. Ma, J. Zhao, Z. Jin, Z. Guo, *Angew. Chem., Int. Ed.* **2020**, *59*, 5151.
[40] S. Y. Guo, Y. P. Zhang, Y. Q. Ge, S. L. Zhang, H. B. Zeng, H. Zhang, *Adv. Mater.* **2019**, *31*, 1902352.
[41] X. H. Liu, S. L. Zhang, S. Y. Guo, B. Cai, S. Y. A. Yang, F. K. Shan, M. Pumera, H. B. Zeng, *Chem. Soc. Rev.* **2020**, *49*, 263.
[42] F. Reis, G. Li, L. Dudy, M. Bauernfeind, S. Glass, W. Hanke, R. Thomale, J. Schafer, R. Claessen, *Science* **2017**, *357*, 287.
[43] S. M. Beladi-Mousavi, A. M. Pourrahimi, Z. Sofer, M. Pumera, *Adv. Funct. Mater.* **2019**, *29*, 1807004.
[44] R. Gusmao, Z. Sofer, D. Bousa, M. Pumera, *Angew. Chem., Int. Ed.* **2017**, *56*, 14417.
[45] C. Kamal, M. Ezawa, *Phys. Rev. B* **2015**, *91*, 085423.
[46] Y. Chen, C. Chen, R. Kealhofer, H. Liu, Z. Yuan, L. Jiang, J. Suh, J. Park, C. Ko, H. S. Choe, J. Avila, M. Zhong, Z. Wei, J. Li, S. Li, H. Gao, Y. Liu, J. Analytis, Q. Xia, M. C. Asensio, J. Wu, *Adv. Mater.* **2018**, *30*, 1800754.
[47] S. Zhang, M. Xie, F. Li, Z. Yan, Y. Li, E. Kan, W. Liu, Z. Chen, H. Zeng, *Angew. Chem., Int. Ed.* **2016**, *55*, 1666.
[48] S. Zhang, Z. Yan, Y. Li, Z. Chen, H. Zeng, *Angew. Chem., Int. Ed.* **2015**, *54*, 3112.
[49] J. Zhao, Z. H. Qi, Y. Xu, J. Dai, X. C. Zeng, W. L. Guo, J. Ma, *Wiley Interdiscip. Rev.: Comput. Mol. Sci.* **2019**, *9*, e1387.
[50] J. Zhao, Y. L. Li, J. Ma, *Nanoscale* **2016**, *8*, 9657.
[51] J. Zhao, W. L. Guo, J. Ma, *Nano Res.* **2017**, *10*, 491.
[52] T. Zhang, Y. Mu, J. Z. Zhao, C. E. Hu, X. R. Chen, X. L. Zhou, *Phys. Chem. Chem. Phys.* **2018**, *20*, 12138.
[53] Y. P. Wang, C. W. Zhang, W. X. Ji, R. W. Zhang, P. Li, P. J. Wang, M. J. Ren, X. L. Chen, M. Yuan, *J. Phys. D: Appl. Phys.* **2016**, *49*, 055305.
[54] Y. Wang, P. Huang, M. Ye, R. Quhe, Y. Pan, H. Zhang, H. Zhong, J. Shi, J. Lu, *Chem. Mater.* **2017**, *29*, 2191.
[55] X. T. Sun, Z. G. Song, S. Q. Liu, Y. Y. Wang, Y. Y. Li, W. Z. Wang, J. Lu, *ACS Appl. Mater. Interfaces* **2018**, *10*, 22363.

[56] G. Pizzi, M. Gibertini, E. Dib, N. Marzari, G. Iannaccone, G. Fiori, *Nat. Commun.* **2016**, *7*, 12585.
[57] E. P. Young, J. Park, T. Bai, C. Choi, R. H. DeBlock, M. Lange, S. Poust, J. Tice, C. Cheung, B. S. Dunn, M. S. Goorsky, V. Ozoliņš, D. C. Streit, V. Gambin, *ACS Appl. Nano Mater.* **2018**, *1*, 4737.
[58] H.-S. Tsai, S.-W. Wang, C.-H. Hsiao, C.-W. Chen, H. Ouyang, Y.-L. Chueh, H.-C. Kuo, J.-H. Liang, *Chem. Mater.* **2016**, *28*, 425.
[59] Z. H. Qi, Y. Hu, Z. Jin, J. Ma, *Phys. Chem. Chem. Phys.* **2019**, *21*, 12087.
[60] B. Liu, M. Kopf, A. N. Abbas, X. Wang, Q. Guo, Y. Jia, F. Xia, R. Weihrich, F. Bachhuber, F. Pielnhofer, H. Wang, R. Dhall, S. B. Cronin, M. Ge, X. Fang, T. Nilges, C. Zhou, *Adv. Mater.* **2015**, *27*, 4423.
[61] E. Kovalska, N. Antonatos, J. Luxa, Z. Sofer, *Inorg. Chem.* **2020**, *59*, 11259
[62] N. Antonatos, V. Mazánek, P. Lazar, J. Sturala, Z. Sofer, *Nanoscale Adv.* **2020**, *2*, 1282.
[63] J. Sturala, A. Ambrosi, Z. Sofer, M. Pumera, *Angew. Chem., Int. Ed.* **2018**, *57*, 14837.
[64] J. Sturala, Z. Sofer, M. Pumera, *NPG Asia Mater.* **2019**, *11*, 42.
[65] H. Yun, S. Ghosh, P. Golani, S. J. Koester, K. A. Mkhoyan, *ACS Nano* **2020**, *14*, 5988.
[66] C. Liu, S. Sun, Q. Feng, G. Wu, Y. Wu, N. Kong, Z. Yu, J. Yao, X. Zhang, W. Chen, Z. Tang, Y. Xiao, X. Huang, A. Lv, C. Yao, H. Cheng, A. Wu, T. Xie, W. Tao, *Adv. Mater.* **2021**, *33*, 2102054.
[67] X. Kong, Q. Liu, C. Zhang, Z. Peng, Q. Chen, *Chem. Soc. Rev.* **2017**, *46*, 2127.
[68] P. Vishnoi, K. Pramoda, C. N. R. Rao, *ChemNanoMat* **2019**, *5*, 1062.
[69] Z. Wu, J. Hao, *npj 2D Mater. Appl.* **2020**, *4*, 4.
[70] A. Zhao, B. Wang, *APL Mater.* **2020**, *8*, 030701.
[71] P. W. Yuan, T. Zhang, J. T. Sun, L. W. Liu, Y. G. Yao, Y. L. Wang, *J. Semicond.* **2020**, *41*, 8.
[72] N. C. Norman, *Chemistry of Arsenic, Antimony and Bismuth*, Springer Science & Business Media, **1997**.
[73] S. Golin, J. A. Stocco, *Phys. Rev. B* **1970**, *1*, 390.
[74] G. N. Greaves, S. R. Elliott, E. A. Davis, *Adv. Phys.* **1979**, *28*, 49.
[75] C. Gao, R. Li, M. Zhong, R. Wang, M. Wang, C. Lin, L. Huang, Y. Cheng, W. Huang, *J. Phys. Chem. Lett.* **2020**, *11*, 93.
[76] K. Luo, S. Y. Chen, C. G. Duan, *Sci. China: Phys., Mech. Astron.* **2015**, *58*, 087301.
[77] P. M. Smith, A. J. Leadbetter, A. J. Apling, *Philos. Mag.* **1975**, *31*, 57.
[78] O. Osters, T. Nilges, F. Bachhuber, F. Pielnhofer, R. Weihrich, M. Schoneich, P. Schmidt, *Angew. Chem., Int. Ed.* **2012**, *51*, 2994.
[79] M. Seidl, G. Balazs, M. Scheer, *Chem. Rev.* **2019**, *119*, 8406.
[80] Y. Hu, X. Wang, Z. Qi, S. Wan, J. Liang, Q. Jia, D. Hong, Y. Tian, J. Ma, Z. Tie, Z. Jin, *Adv. Funct. Mater.* **2021**, 2106529.
[81] J. S. Lannin, *Phys. Rev. B* **1977**, *15*, 3863.
[82] G. N. Greaves, E. A. Davis, J. Bordas, *Philos. Mag.* **1976**, *34*, 265.
[83] W. B. Pollard, J. D. Joannopoulos, *Phys. Rev. B* **1979**, *19*, 4217.
[84] Z. Y. Zhang, J. F. Xie, D. Z. Yang, Y. H. Wang, M. S. Si, D. S. Xue, *Appl. Phys. Express* **2015**, *8*, 055201.
[85] D. Kecik, E. Durgun, S. Ciraci, *Phys. Rev. B* **2016**, *94*, 205410.
[86] P. Vishnoi, M. Mazumder, S. K. Pati, C. N. R. Rao, *New J. Chem.* **2018**, *42*, 14091.
[87] L. Zhao, Q. Xu, X. Wang, J. He, J. Li, H. Yang, Y. Long, D. Chen, H. Liang, C. Li, M. Xue, J. Li, Z. Ren, L. Lu, H. Weng, Z. Fang, X. Dai, G. Chen, *Phys. Rev. B* **2017**, *95*, 115119.
[88] P. Zhang, J. Z. Ma, Y. Ishida, L. X. Zhao, Q. N. Xu, B. Q. Lv, K. Yaji, G. F. Chen, H. M. Weng, X. Dai, Z. Fang, X. Q. Chen, L. Fu, T. Qian, H. Ding, S. Shin, *Phys. Rev. Lett.* **2017**, *118*, 046802.
[89] M. Zeraati, S. M. V. Allaei, I. A. Sarsari, M. Pourfath, D. Donadio, *Phys. Rev. B* **2016**, *93*, 085424.
[90] J. D. Wood, S. A. Wells, D. Jariwala, K. S. Chen, E. Cho, V. K. Sangwan, X. L. Liu, L. J. Lauhon, T. J. Marks, M. C. Hersam, *Nano Lett.* **2014**, *14*, 6964.
[91] J. Shah, W. Wang, H. M. Sohail, R. I. G. Uhrberg, *2D Mater.* **2020**, *7*, 025013.
[92] P. W. Sutter, J. I. Flege, E. A. Sutter, *Nat. Mater.* **2008**, *7*, 406.
[93] A. Fleurence, R. Friedlein, T. Ozaki, H. Kawai, Y. Wang, Y. Yamada-Takamura, *Phys. Rev. Lett.* **2012**, *108*, 025013.
[94] J. D. Zhou, J. H. Lin, X. W. Huang, Y. Zhou, Y. Chen, J. Xia, H. Wang, Y. Xie, H. M. Yu, J. C. Lei, D. Wu, F. C. Liu, Q. D. Fu, Q. S. Zeng, C. H. Hsu, C. L. Yang, L. Lu, T. Yu, Z. X. Shen, H. Lin, B. I. Yakobson, Q. Liu, K. Suenaga, G. T. Liu, Z. Liu, *Nature* **2018**, *556*, 355.
[95] W. L. Lu, H. Y. Nan, J. H. Hong, Y. M. Chen, C. Zhu, Z. Liang, X. Y. Ma, Z. H. Ni, C. H. Jin, Z. Zhang, *Nano Res.* **2014**, *7*, 853.
[96] Q. Q. Ji, Y. Zhang, Y. F. Zhang, Z. F. Liu, *Chem. Soc. Rev.* **2015**, *44*, 2587.
[97] Y. Huang, Y. H. Pan, R. Yang, L. H. Bao, L. Meng, H. L. Luo, Y. Q. Cai, G. D. Liu, W. J. Zhao, Z. Zhou, L. M. Wu, Z. L. Zhu, M. Huang, L. W. Liu, L. Liu, P. Cheng, K. H. Wu, S. B. Tian, C. Z. Gu, Y. G. Shi, Y. F. Guo, Z. G. Cheng, J. P. Hu, L. Zhao, G. H. Yang, E. Sutter, P. Sutter, Y. L. Wang, W. Ji, X. J. Zhou, et al., *Nat. Commun.* **2020**, *11*, 2453.
[98] E. L. Gao, S. Z. Lin, Z. Qinn, M. J. Buehler, X. Q. Feng, Z. P. Xu, *J. Mech. Phys. Solids* **2018**, *115*, 248.
[99] R. T. Lv, J. A. Robinson, R. E. Schaak, D. Sun, Y. F. Sun, T. E. Mallouk, M. Terrones, *Acc. Chem. Res.* **2015**, *48*, 897.
[100] V. Nicolosi, M. Chhowalla, M. G. Kanatzidis, M. S. Strano, J. N. Coleman, *Science* **2013**, *340*, 1226419.
[101] J. N. Coleman, M. Lotya, A. O'Neill, S. D. Bergin, P. J. King, U. Khan, K. Young, A. Gaucher, S. De, R. J. Smith, I. V. Shvets, S. K. Arora, G. Stanton, H. Y. Kim, K. Lee, G. T. Kim, G. S. Duesberg, T. Hallam, J. J. Boland, J. J. Wang, J. F. Donegan, J. C. Grunlan, G. Moriarty, A. Shmeliov, R. J. Nicholls, J. M. Perkins, E. M. Grieveson, K. Theuwissen, D. W. McComb, P. D. Nellist, et al., *Science* **2011**, *331*, 568.
[102] A. Ciesielski, P. Samori, *Chem. Soc. Rev.* **2014**, *43*, 381.
[103] D. Hanlon, C. Backes, E. Doherty, C. S. Cucinotta, N. C. Berner, C. Boland, K. Lee, A. Harvey, P. Lynch, Z. Gholamvand, S. F. Zhang, K. P. Wang, G. Moynihan, A. Pokle, Q. M. Ramasse, N. McEvoy, W. J. Blau, J. Wang, G. Abellan, F. Hauke, A. Hirsch, S. Sanvito, D. D. O'Regan, G. S. Duesberg, V. Nicolosi, J. N. Coleman, *Nat. Commun.* **2015**, *6*, 8563.
[104] C. Backes, T. M. Higgins, A. Kelly, C. Boland, A. Harvey, D. Hanlon, J. N. Coleman, *Chem. Mater.* **2017**, *29*, 243.
[105] P. L. Cullen, K. M. Cox, M. K. Bin Subhan, L. Picco, O. D. Payton, D. J. Buckley, T. S. Miller, S. A. Hodge, N. T. Skipper, V. Tileli, C. A. Howard, *Nat. Chem.* **2017**, *9*, 244.
[106] Z. Zeng, T. Sun, J. Zhu, X. Huang, Z. Yin, G. Lu, Z. Fan, Q. Yan, H. H. Hng, H. Zhang, *Angew. Chem., Int. Ed.* **2012**, *51*, 9052.
[107] J. I. Paredes, S. Villar-Rodil, *Nanoscale* **2016**, *8*, 15389.
[108] X. Xiao, H. Wang, P. Urbankowski, Y. Gogotsi, *Chem. Soc. Rev.* **2018**, *47*, 8744.
[109] M. Naguib, Y. Gogotsi, *Acc. Chem. Res.* **2015**, *48*, 128.
[110] W. J. Zhang, Y. Hu, L. B. Ma, G. Y. Zhu, P. Y. Zhao, X. L. Xue, R. P. Chen, S. Y. Yang, J. Ma, J. Liu, Z. Jin, *Nano Energy* **2018**, *53*, 808.
[111] L. Ma, G. Zhu, D. Wang, H. Chen, Y. Lv, Y. Zhang, X. He, H. Pang, *Adv. Funct. Mater.* **2020**, *30*, 1537.
[112] Y. W. Zhu, S. Murali, M. D. Stoller, K. J. Ganesh, W. W. Cai, P. J. Ferreira, A. Pirkle, R. M. Wallace, K. A. Cychosz, M. Thommes, D. Su, E. A. Stach, R. S. Ruoff, *Science* **2011**, *332*, 1537.
[113] F. Bonaccorso, L. Colombo, G. Yu, M. Stoller, V. Tozzini, A. C. Ferrari, R. S. Ruoff, V. Pellegrini, *Science* **2015**, *347*, 1246501.
[114] C. Gibaja, D. Rodriguez-San-Miguel, P. Ares, J. Gomez-Herrero, M. Varela, R. Gillen, J. Maultzsch, F. Hauke, A. Hirsch, G. Abellan, F. Zamora, *Angew. Chem., Int. Ed.* **2016**, *55*, 14345.

[115] J. F. Shen, Y. M. He, J. J. Wu, C. T. Gao, K. Keyshar, X. Zhang, Y. C. Yang, M. X. Ye, R. Vajtai, J. Lou, P. M. Ajayan, *Nano Lett.* **2015**, *15*, 5449.
[116] J. H. Han, M. Kwak, Y. Kim, J. Cheon, *Chem. Rev.* **2018**, *118*, 6151.
[117] H. L. Chia, N. M. Latiff, R. Gusmao, Z. Sofer, M. Pumera, *Chem. – Eur. J.* **2019**, *25*, 2242.
[118] S. Yang, K. Zhang, A. G. Ricciardulli, P. Zhang, Z. Liao, M. R. Lohe, E. Zschech, P. W. M. Blom, W. Pisula, K. Mullen, X. Feng, *Angew. Chem., Int. Ed.* **2018**, *57*, 4677.
[119] W. Tao, X. Y. Ji, X. B. Zhu, L. Li, J. Q. Wang, Y. Zhang, P. E. Saw, W. L. Li, N. Kong, M. A. Islam, T. Gan, X. W. Zeng, H. Zhang, M. Mahmoudi, G. J. Tearney, O. C. Farokhzad, *Adv. Mater.* **2018**, *30*, 1802061.
[120] Y. Y. Wang, M. Ye, M. Y. Weng, J. Z. Li, X. Y. Zhang, H. Zhang, Y. Guo, Y. Y. Pan, L. Xiao, J. K. Liu, F. Pan, J. Lu, *ACS Appl. Mater. Interfaces* **2017**, *9*, 29273.
[121] S. Yang, Y. Liu, W. Chen, W. Jin, J. Zhou, H. Zhang, G. S. Zakharova, *Sens. Actuators, B* **2016**, *226*, 478.
[122] J. Liu, X. Jiang, R. Zhang, Y. Zhang, L. Wu, W. Lu, J. Li, Y. Li, H. Zhang, *Adv. Funct. Mater.* **2018**, *29*, 1807326.
[123] P. Wan, X. Wen, C. Sun, B. K. Chandran, H. Zhang, X. Sun, X. Chen, *Small* **2015**, *11*, 5409.
[124] Y. Chen, C. L. Tan, H. Zhang, L. Z. Wang, *Chem. Soc. Rev.* **2015**, *44*, 2681.
[125] M. Qiu, W. X. Ren, T. Jeong, M. Won, G. Y. Park, D. K. Sang, L. P. Liu, H. Zhang, J. S. Kim, *Chem. Soc. Rev.* **2018**, *47*, 5588.
[126] X. M. Sun, Z. Liu, K. Welsher, J. T. Robinson, A. Goodwin, S. Zaric, H. J. Dai, *Nano Res.*. **2008**, *1*, 203.
[127] J. T. Robinson, S. M. Tabakman, Y. Y. Liang, H. L. Wang, H. S. Casalongue, D. Vinh, H. J. Dai, *J. Am. Chem. Soc.* **2011**, *133*, 6825.
[128] W. Tao, X. B. Zhu, X. H. Yu, X. W. Zeng, Q. L. Xiao, X. D. Zhang, X. Y. Ji, X. S. Wang, J. J. Shi, H. Zhang, L. Mei, *Adv. Mater.* **2017**, *29*, 1603276.
[129] M. Fortin-Deschenes, O. Waller, Q. An, M. J. Lagos, G. A. Botton, H. Guo, O. Moutanabbir, *Small* **2020**, *16*, 1906540.

Yi Hu received his B.S. degree in Chemistry from Sichuan University in 2014. He received his Ph.D. degree under the supervision of Prof. Zhong Jin in School of Chemistry and Chemical Engineering at Nanjing University. His research interests reside in preparation of 2D nanomaterials and corresponding photoelectrical devices.

Junchuan Liang received his B.S. degree in Lanzhou University in 2019. He is now pursuing his Ph.D. degree under the supervision of Prof. Zhong Jin in School of Chemistry and Chemical Engineering at Nanjing University. His research interests reside in preparation of 2D nanomaterials.

Jing Ma received her B.S and M.S. in Chemistry from Nanjing University of Science and Technology in 1992 and 1995, respectively, and a Ph.D. in Physical Chemistry from Nanjing University in 1998. She is currently a professor of chemistry at Nanjing University. She is primarily interested in developing electronic structure methods and molecular simulation methods and extending their applications to various functional material systems.

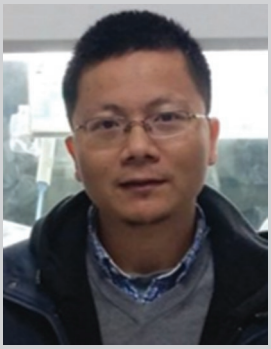

Zhong Jin received his B.S. (2003) and Ph.D. (2008) from Peking University. He worked as a postdoctoral scholar at Rice University (2008–2010) and Massachusetts Institute of Technology (2010–2014). Now he is a professor in School of Chemistry and Chemical Engineering at Nanjing University. Currently, he is leading a research group working on the design and development of advanced materials and device systems for clean energy conversion and storage.